Available online at www.sciencedirect.com
SCIENCE DIRECT
Biochimica et Biophysica Acta 1707 (2005) 51–66
BIOCHIMICA ET BIOPHYSICA ACTA BBA
http://www.elsevier.com/locate/bba

Review

Vibrational spectroscopy to study the properties of redox-active tyrosines in photosystem II and other proteins

Catherine Berthomieu[a,*], Rainer Hienerwadel[b]

[a] CEA-Cadarache, Laboratoire de Bioénergétique Cellulaire, UMR 6191 CNRS-CEA-Aix-Marseille II, Univ.-Méditerranée CEA 1000, Bât. 156, F-13108 Saint-Paul-lez-Durance, Cedex, France
[b] Laboratoire de Génétique et de Biophysique des Plantes, UMR 6191 CNRS-CEA-Aix-Marseille II, Faculté des Sciences de Luminy, Univ.-Méditerranée CEA 1000, 163 Avenue de Luminy, Case 901, 13288 Marseilles cedex, France

Received 27 May 2003; accepted 31 March 2004
Available online 10 May 2004

Abstract

Tyrosine radicals play catalytic roles in essential metalloenzymes. Their properties—midpoint potential, stability. . .—or environment varies considerably from one enzyme to the other. To understand the origin of these properties, the redox tyrosines are studied by a number of spectroscopic techniques, including Fourier transform infrared (FTIR) and resonance Raman (RR) spectroscopy. An increasing number of vibrational data are reported for the (modified-) redox active tyrosines in ribonucleotide reductases, photosystem II, heme catalase and peroxidases, galactose and glyoxal oxidases, and cytochrome oxidase. The spectral markers for the tyrosinyl radicals have been recorded on models of (substituted) phenoxyl radicals, free or coordinated to metals. We review these vibrational data and present the correlations existing between the vibrational modes of the radicals and their properties and interactions formed with their environment: we present that the ν_{7a}(C–O) mode of the radical, observed both by RR and FTIR spectroscopy at 1480–1515 cm^{-1}, is a sensitive marker of the hydrogen bonding status of (substituted)-phenoxyl and $Tyr^{\bullet}$, while the ν_{8a}(C–C) mode may probe coordination of the $Tyr^{\bullet}$ to a metal. For photosystem II, the information obtained by light-induced FTIR difference spectroscopy for the two redox tyrosines Tyr_D and Tyr_Z and their hydrogen bonding partners is discussed in comparison with those obtained by other spectroscopic methods.

Keywords: Photosystem II; Tyrosinyl radical; Phenoxyl radical; Fourier transform infrared (FTIR) spectroscopy; Resonance Raman; Metallo-radical enzymes

1. Introduction

Among the free amino acid radicals identified in proteins, the redox couple tyrosyl radical/tyrosine was shown essential in many biologically important processes (see Ref. [1] for a review). It has been evidenced in key enzymes such as ribonucleotide reductase [2,3], which provides precursors of DNA synthesis, and photosystem II (PSII) [4,5]—the membrane protein complex where photosynthetic oxygen evolution takes place in plants, algae and cyanobacteria.

Ribonucleotide reductase: In class I ribonucleotide reductase (RNR), the redox active Tyr_{122} (amino acid numbering according to *E. coli* sequence) is located at 5–6 Å of the di-iron cluster on the R2 subunit (Fig. 1A) [6]. The $Tyr^{\bullet}$ is generated upon reduction of oxygen into water at the iron cluster (Ref. [7] and references therein). $Tyr^{\bullet}$ initiates the formation of a thiyl radical at the active site for ribonucleotide reduction on the R1 subunit. This thiyl radical, proposed to occur on Cys_{439}, in turn initiates catalysis on the nucleotide substrate [7–10].

Photosystem II: In PSII, two redox tyrosines, Tyr_D and Tyr_Z, have been evidenced, at homologous positions on the two polypeptides D2 and D1 forming the core of the membrane protein complex (reviewed in Refs. [11–13]). Light absorption at a chlorophyllic species so-called primary electron donor P_{680} induces a charge separation between P_{680} and an electron acceptor plastoquinone Q_A. Tyr_Z and/or Tyr_D reduce the highly oxidizing P_{680}^{+}, generating the Tyr radicals. Tyr_Z is located at ≈ 7 Å of the Mn_4-Ca^{2+} active center for oxygen evolution [14–18]. Tyr_Z is directly

* Corresponding author. Tel.: +33-4-4225-4353; Fax: +33-4-4225-4701.
E-mail address: catherine.berthomieu@cea.fr (C. Berthomieu).

0005-2728/$ - see front matter © 2004 Elsevier B.V. All rights reserved.
doi:10.1016/j.bbabio.2004.03.011

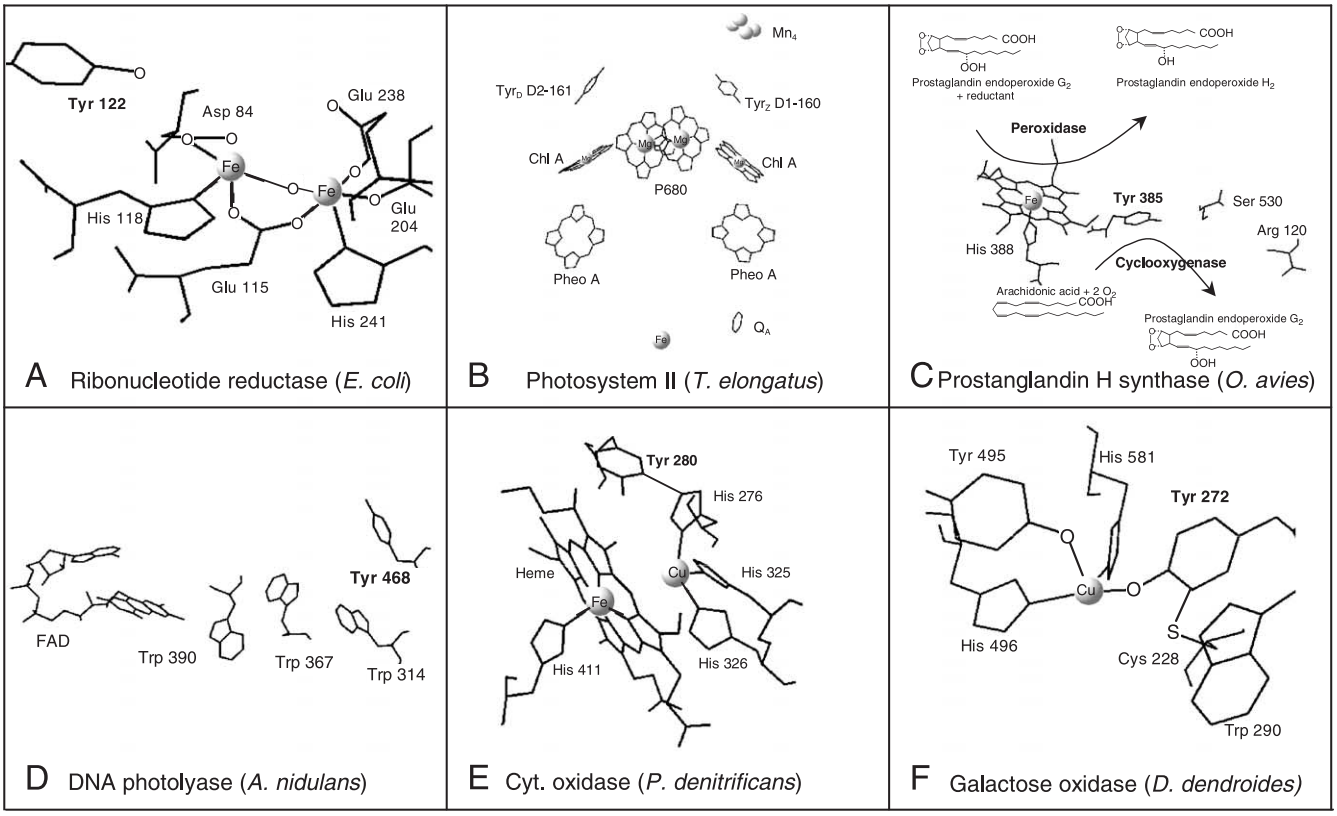

Fig. 1. Scheme of the Tyr• environment in (A) class I ribonucleotide reductase (modified from Ref. [6]), (B) photosystem II [16–18], (C) prostaglandin H synthase [151], (D) DNA photolyase of *A. nidulans* [152] with postulated Trp and Tyr residues involved in the electron-transfer reaction. (E) His-Tyr• at the Cu_B-Heme a3 of cytochrome *c* oxidase [35] and (F) cysteinyl-Tyr• at the active site of galactose oxidase or glyoxal oxidase [46].

involved in the physiological electron and proton transfer reactions associated with water oxidation into molecular oxygen (Fig. 1B, see below). Tyr_D is not essential for oxygen evolution. However, mutation of this strictly conserved redox tyrosine in the obligatory photoautotrophic *Thermosynechoccocus* species largely increases the growth generation time and tendency to revert [M. Sugiura et al. in preparation]. The interactions of Tyr_D with the Mn-Ca^{2+} cluster and P^{+}_{680} are reviewed in Ref. [19].

Stable or transient tyrosine radicals are also implicated in a variety of regulatory enzymes that are important in primary metabolism.

Prostaglandin synthases: Prostaglandin synthases are essential for the production of a variety of prostaglandins from arachidonic acid. This process implies both a cyclooxygenase reaction, which converts arachidonic acid to prostaglandin G_2, and the hydroxylation of prostaglandin G_2 into prostaglandin H_2 (Fig. 1C). This latter peroxidation reaction involves a highly oxidizing intermediate so-called compound I, an oxoferryl protoporphyrin IX radical cation ($FeIV{=}O\ PPIX^{+}$ •) [20,21] that generates Tyr• by intraprotein electron transfer. Tyr• in turn initiates the cyclooxygenase reaction by forming the arachidonate radical [22,23] which reacts with oxygen to yield prostaglandin G2. Crystallographic data revealed that the Tyr• would be located between the heme and arachidonate binding sites, well positioned to couple the two enzyme activities [24].

Catalases and peroxidases: More generally, for most catalases and peroxidases having a protoporphyrin prosthetic group at the active site, the highly oxidizing compound I or, alternately, an oxoferryl protoporphyrin IX and a protein-based radical species are generated by the two-electron oxidation of the protoporphyrin by alkhyl- or hydrogen-peroxides [25]. A Trp• intermediate relevant for substrate oxidation was observed for cytochrome *c* peroxidase [26], while formation of an oxoferryl protoporphyrin IX-Tyr• intermediate was evidenced in beef liver catalase [27], turnip and cytochrome *c* peroxidases [28,29] and catalase-peroxidases from *Mycobacter tuberculosis* and *Synechocystis* [30,31].

DNA photolyase and cryptochrome-1: Finally, an electron transfer from a tyrosine residue to a tryptophane radical was detected in the DNA photolyase of *Anacystis nidulans* [32] (Fig. 1D), while tryptophane radicals only were detected in the same enzyme of *E. coli* [33]. DNA photolyases are flavoproteins that catalyze UV-induced repair of major UV-damaged DNA lesions by reduction of pyrimidine dimers. Recently, a transient Tyr• was also detected in the blue light photoreceptor cryptochrome-1 from *Arabidopsis thaliana* [34] which shows large sequence homology with DNA-photolyase.

1.1. Modified redox active tyrosines

Redox active modified tyrosines are also implicated in a number of metallo-radical enzymes, which couple substrate oxidation with oxygen reduction into H_2O_2 or water.

Cytochrome oxidase: In cytochrome oxidase, the terminal enzyme in the respiratory chain of the mitochondria, as well as in other heme-copper terminal oxidases, the active site for oxygen reduction is located at a binuclear metal center formed by a high-spin heme A (heme a3) and copper Cu_B [35–38] (Fig. 1E). A tyrosine, which forms a covalent bond to an histidine ligand of Cu_B [35,36], was shown to be redox-active by $^{125}I^-$ labeling and peptide mapping analysis [39]. The His-Tyr$^\bullet$ was also observed during the reaction of the heme-copper oxidases with H_2O_2 [40,41].

Galactose and glyoxal oxidases: Thioether-Tyr, resulting from the covalent binding of the sulfur atom of adjacent cysteine at the α position of the phenol ring, was identified at the active site of galactose oxidase [42–44] and glyoxal oxidase [45]. Glyoxal oxidase is a fungal enzyme and the physiological partner of lignin peroxidase and Mn peroxidase. It couples the oxidation of a number of aldehydes and α-hydroxy carbonyl compounds with the reduction of O_2 to H_2O_2. Galactose oxidase catalyzes the two-electron oxidation of primary alcohols to aldehydes with the concomitant reduction of dioxygen to hydrogen peroxide. Although dissimilar in primary sequence, the two enzymes have very similar active sites, in which the modified tyrosine directly coordinates to the active site copper ion [46] (Fig. 1F). Catalysis implies redox reactions of both the copper and cysteinyl-Tyr ligand (Ref. [47] and references therein).

Copper amine oxidase: In copper amine oxidase, the 2,4,5-trihydroxyphenylalanine quinone or topaquinone TPQ cofactor results from a posttranslational copper-dependent oxidation of a conserved tyrosine residue [48,49]. This TPQ forms a transient iminosemiquinone radical during the enzyme turnover.

1.2. A specific role for tyrosine?

The tyrosine radicals are crucial for the redox reactions catalyzed by these enzymes, as demonstrated for some of them using site-directed mutagenesis or specific labeling [1,12,13,21]. The specific role of tyrosine as compared to other possible redox cofactors is, however, not fully understood. Except for the transient Tyr$^\bullet$ evidenced in DNA-photolyase or cryptochrome and for Tyr_D in PSII, the Tyr$^\bullet$ are generated during metal- and oxygen or H_2O_2-mediated transformations [9,12,20,25,40,47]. A specific role for radical chemistry, i.e. homolytic cleavage of C–H, S–H, or O–H bonds, which involves coupled electron and proton transfer reactions, in contrast to pure electron transfer reactions, and the involvement of high midpoint potentials have been proposed.

In ribonucleotide reductase, the Tyr$^\bullet$ di-iron site on R2 and the active site for ribonucleotide reduction on R1 are separated by 35 Å. Long-range electron transfer between these two sites was demonstrated using an enzyme inhibitor [50,51]. Conserved tryptophane and tyrosines between the redox Tyr_{122} and Cys_{439} could serve as redox intermediates. The occurrence of pure electron transfer, concerted electron and proton transfer, or hydrogen atom transfer is debated. Discontinuity in hydrogen-bonded paths between Tyr_{122} and Cys_{439} is not in support of a hydrogen atom transfer mechanism. Local coupling of proton/electron transfer is proposed to occur during the reaction cycle, notably for Cys_{439} oxidation to meet the thermodynamic requirements of its oxidation by Tyr$^\bullet$, while other steps might solely involve "classical" electron transfer, followed by proton release/uptake [1,9].

In galactose oxidase, oxidation of the substrate alcohol involves a two-electron oxidation, deprotonation and the cleavage of one of the Cα–H bonds within the hydroxymethylene group. This occurs through oxidation of the copper, protonation of the tyrosinate Cu ligand and cleavage of the Cα–H bond by the cysteinyl-Tyr ligand. The strong kinetic isotope effect associated with the oxidation of $C_\alpha{}^1H$- or $C_\alpha{}^2H$-labeled substrates and the strong temperature dependence of this effect were interpreted in favor of a hydrogen atom abstraction mechanisms from the substrates by the coordinated cysteinyl-Tyr$^\bullet$ radical [52,47]. For prostaglandin H synthase, and for Tyr_Z of PSII, direct involvement in the oxidation of the substrate arachidonic acid [20] or Mn-bound water or hydroxyl [52–56] was proposed, through (concerted) proton and electron abstraction from C–H or O–H bonds.

Detailed analysis of the properties of the Tyr$^\bullet$/Tyr redox couples should help clarify the advantages of using (modified) tyrosines in catalysis. The elucidation of the structural parameters at the origin of their specific properties in each enzyme is determinant. Indeed, the properties of these redox active tyrosines, their midpoint potential, the stability or reactivity of the radical, largely vary from one enzyme to the other, or within the same enzyme, as exemplified by the two redox-active tyrosines in PSII [11–13]. In practice, it would be useful to correlate the spectroscopic characteristics of the redox-active tyrosines with their specific properties and with the characteristics of their environment, such as their hydrogen bonding interactions. Vibrational spectroscopy, which probes directly the properties of chemical bonds, is specially suited to detail the chemical properties of the redox tyrosines and to address the main issue of the hydrogen bonding status of the tyrosine radicals.

In the following, we summarize the different hypotheses formulated for the oxidation mechanism of the two redox active tyrosines of PSII. We compare the methodology of Fourier transform infrared (FTIR) and resonance Raman (RR) spectroscopy and analyze the principal diagnostic vibrational modes reported for tyrosine radicals and phenoxyl derivatives. The vibrational data on redox tyrosines in proteins and notably in PSII are summarized and are

compared with those obtained by other spectroscopic techniques, such as high-field EPR (HF-EPR), ESEEM, and ENDOR spectroscopy, to describe the properties of the tyrosinyl radicals. We also underline the specific information obtained using FTIR difference spectroscopy concerning the pK_A and interactions formed by reduced tyrosine and its environment.

2. Redox active tyrosines in photosystem II

PSII is a transmembrane protein that carries out the initial steps of oxygenic photosynthesis. Water oxidation into molecular oxygen takes place at the so-called "oxygen evolving complex" (OEC), containing four Mn and one Ca^{2+} [11–13,57–59, for recent reviews]. The sequential accumulation of four oxidizing equivalents at the OEC corresponds to five oxidation states denoted S_0 to S_4. Molecular oxygen is released upon the S_4-to-S_0 transition. The mechanism of water oxidation is not well understood [12,13]. It was first underlined that Tyr_Z plays a role in the stabilization of the $P_{680}^{+}Q_A^{-}$ charge-separated state, as compared to charge recombination [11]. More recently, it was proposed that the redox couple $Tyr_Z^{\bullet}/Tyr_Z$ takes part directly in water oxidation [14,15,53,55,60]. The large difference in pK_A for reduced and radical tyrosines led to the conclusion that deprotonation accompanies radical formation. The relative flexibility of $Tyr_Z^{\bullet}$ observed in Mn-depleted PSII suggested that different chemical groups may be involved as proton acceptor and donor upon Tyr_Z oxidoreduction. In addition, the short distance between Tyr_Z and the Mn cluster, the comparison of OH bond dissociation energies for Mn-bound water or hydroxyl and TyrOH, and the thermodynamic advantage to oxidize the Mn_4Ca-cluster maintaining a constant charge in the complex are some of the experimental results and arguments put forward for the possible role of Tyr_Z as $H^{\bullet}$ abstractor from the Mn-bound substrate or as electron acceptor from the Mn_4Ca-cluster and of a proton from the bound water (Refs. [14,15,55,60]).

Alternately, (i) the oscillating behavior of proton release in the lumen upon S-state transitions [61–63], (ii) the electrochromic shift of the absorption band of a chlorophyll of P_{680}, coincident with the lifetime of $Tyr_Z^{\bullet}$ [64], as well as (iii) the effect of pH and $^1H/^2H$ exchange on the electron transfer kinetics between Tyr_Z and P_{680}^{+} [63,65–67] suggested that the oxidation of Tyr_Z coincides with a proton transfer to a nearby acceptor B, creating an uncompensated charge in the vicinity of P_{680}. The reduction of $Tyr_Z^{\bullet}$ in oxygen evolving PSII could result from pure electron transfer from the Mn cluster and restitution of the proton by the base BH. The recent three-dimensional structure of PSII showed that D1-His190 could be this base (see below) [18].

Different oxidation/reduction mechanisms of Tyr_Z, modulated by the oxidation-state of the Mn cluster cannot be excluded from the available experimental data [14,15,56,63]. In particular, it was proposed that the S_1-to-S_2 oxidation step, occurring at temperatures as low as 140 K, is not compatible with the large proton or protein motions stemming from the (concerted) electron and proton abstraction model [56]. In contrast, $H^{\bullet}$ abstraction could be the limiting step during the S_3-to-S_0 transition resulting in oxygen evolution [68] (reviewed in Ref. [63]).

A better understanding of the mechanism of Tyr_Z oxidation in both Mn-depleted and oxygen evolving PSII requires the analysis of the parameters that determine its optical, magnetic and vibrational signatures. In this respect, the comparison of experimental data obtained on the two redox-active tyrosines Tyr_Z and Tyr_D of PSII is very useful. Briefly, EPR, ESEEM and ENDOR (or ESE-ENDOR) spectroscopies on PSII WT and mutants showed that the two $Tyr^{\bullet}$ present very similar spin distribution, but different hydrogen bonding pattern (reviewed in Refs. [12,13]). $Tyr_D^{\bullet}$ forms a well-defined hydrogen bond to D2His189 in spinach or two hydrogen bonds (to D2His189 and possibly D2Gln164) in *Synechocystis* (*Synechocystis* numbering) [12,13,69–72]. It is generally accepted that D2His189 is the proton-accepting base upon $Tyr_D^{\bullet}$ formation. The interactions formed by $Tyr_Z^{\bullet}$ and the homologuous histidine on the D1 polypeptide (D1His190) are under debate [12,54], while the role of D1His190 as proton acceptor upon $Tyr_Z^{\bullet}$ formation was demonstrated in Mn-depleted PSII (reviewed in [12,13]). The recent crystallographic data obtained on photosystem II from the cyanobacterium *Thermosynechococcus elongatus* indicated a hydrogen bond between Tyr_Z and D1His190 [18].

In Mn-depleted PSII, the electron transfer kinetics between Tyr_D and Tyr_Z and the oxidized primary donor P_{680}^{+} are identical at high pH (pH>7.5), but differ by a factor of 10 000 at pH below 7, the reduction of P_{680}^{+} by Tyr_D being largely slowed down [73,74]. The drastic effect of pH on the kinetic of Tyr_D oxidation titrates with an apparent pK_A of 7.7 [74], which seems also to determine the efficiency of Tyr_D oxidation at low temperature [75]. Restricted proton transfer is expected at cryogenic temperature and it was proposed that this pK_A is either that of reduced Tyr_D or that of the D2His189 distal nitrogen [75].

In oxygen evolving PSII, the predominant nanosecond phases of Tyr_Z oxidation by P_{680}^{+}, sensitive to $^1H/^2H$ instead of H/D exchange, decrease at pH below 7 [76]. This was assigned to a restricted proton transfer from Tyr_Z to D1His190, inhibited at pH below 6 by D1His190 protonation [76]. The ability to oxidize Tyr_Z at low temperature also depends on pH, with an apparent pK_A at $\approx$ 5.5 in Mn-depleted PSII [77]. In Mn-depleted PSII core complexes, the disappearance at high pH of the large deuterium kinetic isotope effect of $Tyr_Z^{\bullet}$ formation was assigned to the deprotonation of Tyr_Z, with a pK_A of 8.5 in WT PSII [65,67] or 10.5 in the D1His190Ala mutant [66].

The molecular origin of the pH dependence of Tyr_D and Tyr_Z oxidation kinetics is a key question to better understand the function of PSII, as well as the implication of the

histidines in hydrogen-bonding networks and the localization of the proton released upon $Tyr^{\bullet}$ formation.

3. RR and FTIR studies of phenoxyl and tyrosyl radicals

RR and FTIR spectroscopies have been used to evidence the presence of $Tyr^{\bullet}$ radicals in proteins and to probe the properties of these radicals, e.g. their hydrogen-bonding status [2,41,45,78–83]. This implies that spectral markers for structural and electronic properties of these radicals are identified. To this aim, the vibrational signatures of $Tyr^{\bullet}$ in proteins are compared with spectra recorded with model compounds [84–102]. We review the data reported on (modified) phenoxyl model compounds and $Tyr^{\bullet}$ by RR and infrared spectroscopy and the influence of hydrogen bonding interaction, solvent polarity or coordination to a metal on the vibrational modes of these radicals.

RR and FTIR spectroscopies give complementary information regarding the vibrational properties of the $Tyr^{\bullet}/Tyr$ redox couple (see below). Their experimental utilization is also different. RR spectroscopy can probe the $Tyr^{\bullet}$ radical selectively, by the enhancement of vibrational modes related to the phenoxyl $\pi \rightarrow \pi^*$ (electronic) transition at $\approx$ 410 nm. In contrast, FTIR spectroscopy is not selective and all vibrations from the protein and cofactors will contribute to the infrared absorption spectrum. Also, for experiments performed in transmission mode, the high absorption of the aqueous buffer limits the FTIR sample thickness below 10 μm and implies the use of highly concentrated protein samples (Fig. 2A).

No information on specific residues or active sites are obtained directly from the infrared absorption spectrum of a protein. FTIR difference spectra between the absorption of the reduced and the radical state must be analyzed [103,104]. The radical must be generated rapidly on the sample without any perturbation such as dilution, change in temperature, or pH. The IR modes of phenoxyl or tyrosinyl radicals in aqueous buffer were first obtained by UV-irradiation at low temperature (Fig. 2C) [92–94]. Recently, electrochemistry coupled to ATR-FTIR spectroscopy was used to generate the relatively stable 2,4,6-tri-substituted phenoxyl radicals [102]. In PSII, the FTIR difference spectra were obtained photochemically (Fig. 2B). For sam-

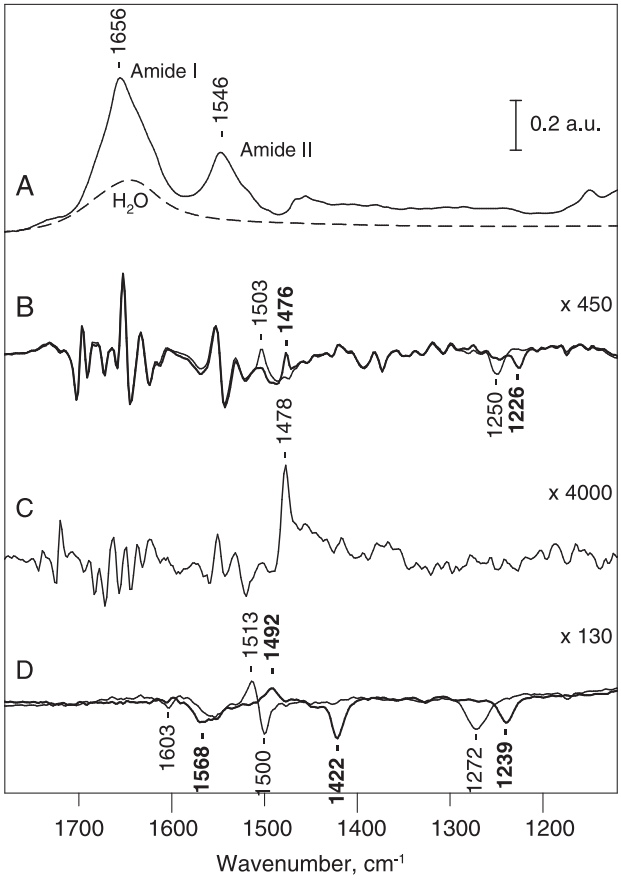

Fig. 2. Reaction-induced FTIR difference spectroscopy. (A) Infrared absorption spectrum of a concentrated pellet of PSII enriched membranes from spinach deposited between two CaF_2 windows, with a path length below 10 μM. This spectrum is dominated by contributions of the polypeptide backbone, with the peptide ν(C=O) amide I mode between 1700 and 1620 cm^{-1}, and the ν(CN)+δ(NH) amide II mode maximum at $\approx$ 1546 cm^{-1}. The contribution of the aqueous buffer in the sample is evaluated by the spectrum with dashed line, maximum at $\approx$ 1640 cm^{-1}. The sample absorption is kept below 0.9 absorption units to avoid spectral distortions induced by the non-linear response of the MCT detector for strongly absorbing samples. (B) Superimposition of the $Tyr_D^{\bullet}/Tyr_D$ FTIR difference spectra obtained with PSII core samples from *Synechocystis* sp. PCC 6803 unlabeled (thin line) or with $^{13}C_1$(4)-labeled tyrosine (bold line) [82]. Negative bands correspond to the dark-adapted state (Tyr_D-state), positive bands to the light-induced state ($Tyr_D^{\bullet}$-state). As compared to the absorption spectrum, the difference spectra induced by UV–Vis light are enlarged by factors of 100 to 5000 to visualize the thin bands, which are highly reproducible provided the sample temperature and integrity remain unchanged during the reaction. Single vibrators, selectively perturbed at active sites in a protein, contribute to the difference spectra. Note that in the $Tyr_D^{\bullet}/Tyr_D$ FTIR difference spectra, mainly one positive band at 1503 cm^{-1} and one negative band at 1250 cm^{-1} are clearly downshifted to 1476 and 1226 cm^{-1}, respectively, in the spectrum recorded with the PSII sample containing $^{13}C_1$(4)-Tyr. This demonstrates the involvement of the tyrosine CO group at these frequencies. The almost perfect superimposition of the spectra in the whole spectral range at the exception of these frequencies, together with the clear determination of the signal downshifts, guarantees the quality of the data. (C) Q_A^-/Q_A FTIR spectrum recorded with PSII enriched membranes of spinach [81]. (D) UV-induced $Tyr^{\bullet}/Tyr^-$(thin line) and ^{2}H ring labeled $^2H_4Tyr^{\bullet}/^2H_4Tyr^-$(bold line) FTIR spectra. The negative bands correspond to the tyrosinate IR modes perturbed upon radical formation. The positive bands correspond to the UV-induced $Tyr^{\bullet}$. The downshift by $\approx$ 78 cm^{-1} induced by the Tyr ring ^{2}H labeling on the negative band at 1500 cm^{-1} is in total agreement with the assignment of this band to the ν_{19}(C–C) mode of tyrosinate. The much smaller shift of – 21 cm^{-1} observed for the positive band at 1513 cm^{-1} (shifted to 1492 cm^{-1}) reliably excludes that this signal corresponds to a tyrosine ring ν(C–C) mode. In contrast, this downshift together with the downshift by 37 cm^{-1} of this positive band upon ring $^{13}C_6$ labeling (not shown, Ref. [93]) are very close to those predicted by normal mode calculations on the radical for the ν(C–O) IR mode of $Tyr^{\bullet}$ (Ref. [93] and references therein). The labeling studies are a strong argument to show that formation of $Tyr^{\bullet}$ and not perturbation (or protonation) of tyrosinate was obtained by the UV-photochemistry performed at 40 K for the tyrosinate sample in borate buffer at pH 11 [92,93].

Table 1
Main vibrational modes of phenoxyl derivatives

	ν(C–C), *Argon*	ν_{7a}(C–O), *Argon*	ν_{19b}(C–C), *Argon*	ν_{19a}(C–C), *Argon*	ν_{9a}(C–C), *Argon*
PhO$^{\bullet}$	1552, *1550*	1504, *1481*	*1515*	1406–1398, *1397*	1163–1157, *1167*
2,4,6-Tri-*tert*-butyl-PhO$^{\bullet}$	1573	1505			
2,6-Di-*tert*-butyl-4-methoxy-PhO$^{\bullet}$	1592	1511–1509			
Metal-coordinated 2,6-di-*tert*-butyl-4-methoxy-PhO$^{\bullet}$	1628–1614	1520–1494			
p-Methoxy-PhO$^{\bullet}$	1607				
p-Methyl-PhO$^{\bullet}$	1574	1513	1537		
p-Ethyl-PhO$^{\bullet}$	1574	1515			
Tyr$^{\bullet}$	1577	1513	1535		
Cys-Tyr$^{\bullet}$	1587	1530			
Metal-coordinated 2,SCH_3-*para*-*tert*-buthyl-PhO$^{\bullet}$	1595–89	1517–12			
Glyoxal/galactose oxidase	1595–91	1487–6			
2-Imidazol-phenoxyl	1587	1530			

These data summarize some of the results described in Refs. [81,84–100,102,112,113]. The data in italics correspond to IR modes of PhO$^{\bullet}$ obtained in an argon matrix.

ples with absorption maxima of up to 0.9 a.u., the difference spectra show IR absorbance changes of 10^{-6} to 10^{-3} a.u. corresponding to single IR modes. (see Fig. 2 for details on the technique).

In these difference spectra, IR modes from both the radical and resting states are obtained. In proteins, FTIR difference spectroscopy brings thus information on the reduced tyrosines, for example Tyr_D and Tyr_Z in PSII [78,81–83] or His-Tyr in cytochrome *c* oxidase [105,106]. The pK_A and hydrogen-bonding status of reduced Tyr can be deduced from their IR modes [82]. FTIR difference spectroscopy can also be used to identify neighboring amino acids perturbed by Tyr oxidation, and their implication in hydrogen bonding interaction or as proton acceptor (donor).

4. Uncoordinated radicals

The characteristic IR and Raman frequencies of radicals from tyrosine or simplified models, phenol, *p*-methyl or *p*-ethyl phenol, have been recorded on unlabeled or specifically ^{2}H-, ^{13}C-, ^{17}O- and ^{18}O-labeled compounds. The radicals were generated chemically, electrochemically, or by UV-photochemistry at ambient or cryogenic temperature in aqueous buffer [81,84–95,102] and recently in argon matrix [96]. These data show that RR and IR modes may be used as markers of the interactions of the radical with its environment.

4.1. ν7a(C–O) mode

RR spectra of phenoxyl or Tyr radicals in (frozen) solution are characterized by an intense mode at 1498–1515 cm^{-1} identified as the ν_{7a}(C–O) mode using ^{17}O-labeling [84–91].

The FTIR difference spectra of (*p*-substituted) phenol or tyrosine radicals obtained by UV photochemistry at low temperature (77–40 K) in borate buffer (Fig. 2D) [81,92,93] show that the radicals contribute one predominant IR mode at 1504 cm^{-1} for phenoxyl and at ≈ 1515 cm^{-1} for Tyr$^{\bullet}$ or *p*-methyl-phenoxyl [81,92,93]. This signal was assigned to the ν_{7a}(C–O) mode, according to its sensitivity to ring ^{2}H-, ring ^{13}C-, and ^{18}O-isotope labeling [92,93], as reported by RR spectroscopy. A similar assignment was proposed for the signal detected at 1516–1510 cm^{-1} in radical-minus-reduced FTIR difference spectra recorded with tyrosinate (Fig. 2D) and a series of X-Tyr and Tyr-X di-peptides, although the downshift upon specific $^{13}C_1$(4)-labeling could not be detected in these dipeptides [94].[1] Finally, the ν_{7a}(C–O) mode was reported at 1505 and 1509 cm^{-1} for 2,4,6-tri-*tert*-butylphenoxyl and 2,6-di-*tert*-butyl-4-methoxyphenoxyl, respectively [102] (Table 1).

The abovementioned studies on models were all performed in strongly interacting environments. In contrast, Spanget-Larsen et al. [96] reported IR modes of the phenoxyl radical and of its labeled derivatives generated in an argon matrix, devoid of possible electrostatic or hydrogen-bonding interactions. The radicals were generated by UV-irradiation, at 308 nm, of nitrosobenzene or nitrobenzene. An intense IR mode was observed at 1481 cm^{-1}. The frequency downshifts of this mode upon $^{2}H_5$- and $^{13}C_1$(4)-phenol labeling

[1] The sample concentration may be critical to obtain reliable UV-induced FTIR difference spectra of phenoxyl derivatives. π-Stacking, electrostatic, and/or hydrogen bonding interactions between phenol or tyrosine molecules in solution were observed by NMR for concentrations greater than 10 mM [93]. To avoid IR signals consecutive to changes in these interactions, in addition to the IR modes of the radical itself in radical-minus-reduced FTIR difference spectra, concentrations were fixed at 10 mM in Ref. [93]. The 10 times larger concentrations (100 mM) used in the work by Ayala et al. [94] or Cappuccio et al. [95], may well increase the signal-to-noise in the UV-induced FTIR difference spectra but also introduce IR contributions not directly related to radical formation. The effect of Tyr concentration on these spectra should be studied, notably as regards the interpretation of changes in the amine NH force constant upon radical formation. These changes may be due to inter molecular interactions in the samples rather than to an intramolecular interaction between the π system of the tyrosyl radical and the amino group [94].

(−14 and −26 cm^{-1}, respectively) were in agreement with those observed for the ν_{7a}(C−O) mode of PhO• at 1505 cm^{-1} (≈ −15 cm^{-1} for $^{2}H_5$-PhO•) or that of Tyr• at 1513 cm^{-1} in frozen solutions (−21 and −29 cm^{-1}, respectively) [85,86,90,92,93]. These data thus demonstrate that the ν_{7a}(C−O) mode of PhO• contributes at 1481 cm^{-1} for the radical generated in argon matrix. This is a strong experimental evidence for the sensitivity of the ν_{7a}(C−O) mode frequency to the environment of the (substituted)phenoxyl radicals. The polarity of the medium substantially increases the frequency of the ν_{7a}(C−O) mode up to 24 cm^{-1}.

4.2. v8a(C−C) mode

The second larger mode detected by RR spectroscopy at 1550–1585 cm^{-1} was assigned to dominant ring C_{ortho}–C_{metha} vibration, denoted ν_{8a}(C−C) [84–91]. The frequency and intensity of this mode is sensitive to ring substituents in *para* position and to the coordination of the phenoxyl radical to a metal (see below, [86,91,97–101]). This mode is reported at 1577 cm^{-1} for *p*-methyl-phenoxyl and 1565 cm^{-1} for Tyr• by RR [86,89]. It contributes at 1606 cm^{-1} for *p*-methoxy-phenoxyl [86] and as a strong band at 1592 cm^{-1} for 2,6-di-*tert*-butyl-4-methoxyphenoxyl [102]. In the FTIR spectrum of PhO• generated in an argon matrix [96], this mode is reported at 1550 cm^{-1}, indicating that it is not a sensitive marker of the polarity of the environment for phenoxyl. A very weak IR signal at 1593–1585 or 1577 cm^{-1} for Tyr• [93,94] and at 1574 cm^{-1} for *p*-methyl-phenol• [93] was also tentatively assigned to this mode (Table 1).

4.3. Other modes

In the 1800–1000 cm^{-1} region, low-intensity signals at 1398–1406 and 1163–1157 cm^{-1}, sensitive to phenoxyl ^{17}O- and/or $^{13}C_6$-labeling, have been assigned to the ν_{19a}(C–C) and ν_{9a}(C−C) modes by RR spectroscopy [90]. These modes were not detected by infrared spectroscopy for PhO• in solution. They were reported at 1397 and 1167 cm^{-1} for the phenoxyl• generated in an argon matrix [96] and do not seem to be useful markers of the interactions formed by Tyr• in proteins. In contrast, bands of low intensity detected at 1535–1537 cm^{-1} for Tyr• and *p*-methyl-phenol• in solution but also observed upon $Tyr_Z^{\bullet}$ and $Tyr_D^{\bullet}$ formation in PSII [78,82,93] may correspond to the IR ν_{19b}(C−C) mode observed at 1515 cm^{-1} for non-interacting PhO• in an argon matrix [96]. This mode of moderate intensity, sensitive to $^{2}H_5$-phenol labeling but insensitive to $^{13}C_1$(4)-labeling, may be a useful infrared marker of the interactions formed by Tyr• in proteins. Further experimental data, however, are needed to confirm this possibility.

Finally, strong IR bands characterize the radicals at frequencies below 1000 cm^{-1}, at 898, 784, and 635 cm^{-1} [96]. The presence of an IR mode at ≈610 cm^{-1}, sensitive to ^{18}O-labeling, could explain the origin of the combination band detected by FTIR at 2110 cm^{-1} for PhO• in solution, and downshifted by 26 cm^{-1} for ^{18}O-labeled phenoxyl [92,93].

The mode assignments described above result from the effect of isotope labeling and from predictions performed by theoretical calculations. Ab initio and density functional quantum chemical calculations reproduce relatively correctly both the experimentally determined frequencies and isotope shifts for Tyr• and phenoxyl radicals [90,96,100,107–109]. Schnepf et al. [100] underlined that only the ν_{7a}(C−O) mode exhibited a serious deviation from the experimentally determined frequency. This mode was calculated at lower frequencies than observed and its frequency did not follow the trend predicted upon increasing quinoïd character of the CO bond in $H < CH_3 < CH_3O^-$ *para*-substituted PhO•. It was therefore suggested that the ν_{7a}(C−O) mode is particularly sensitive to the molecular environment of the oxygen. Calculations performed on isolated and hydrogen-bonded phenoxyl predicted an upshift by 29 cm^{-1} of the ν_{7a}(C−O) vibration frequency upon hydrogen bonding to two water molecules [110]. Comparison of the IR data by Spanget-Larsen et al. [96] and those obtained in aqueous buffer [84–94] nicely demonstrates experimentally the sensitivity of this mode to the polarity of the environment.

5. RR data on metal-phenoxyl complexes and related enzymes

Metal coordinated radicals reveal a similar band pattern as the free radicals with the ν_{8a}(C−C) and ν_{7a}(C−O) modes dominating the RR spectra. However, comparison of the RR spectra recorded with free or Ga-, Sc-, Fe-, Zn- or Cu-coordinated 2,6-di-*tert*-butyl-4-methoxyphenoxyl radical showed that coordination to these metals induces a significant frequency increase of the ν_{8a}(C−C) mode from 1590 cm^{-1} to 1614–1628 cm^{-1} [98–100,102]. The ν_{8a}(C−C) mode intensity is also largely enhanced by excitation in the $\pi \rightarrow \pi^*$ transition in these complexes and the ν_{7a}/ν_{8a} intensity ratio is reversed for the metal-coordinated versus free radical [98–100] (see, however, Ref. [102]). The upshift of the ν_{8a}(C−C) may reflect the shortening of the C_{ortho}–C_{para} bond, i.e. the increased semiquinoïd structure of the radical.

The frequency of the ν_{7a}(C−O) mode in these complexes, comprised between 1494 and 1520 cm^{-1}, as compared to 1511–1509 cm^{-1} for the free radical, does not follow the same trend. The ν_{8a}(C−C)−ν_{7a}(C−O) frequency difference was taken as an empirical measure of the electron withdrawing capacity of the metal (i.e. the increased π character of the Metal···O bond). This frequency difference also correlates with the midpoint potential of the phenoxyl/phenolate couple for *p*-methoxy-substituted phenoxyls [100]. In contrast, for 2,4-di-*tert*-butyl-phenoxyl radicals coordinated to a series of alkaline earth metal ions and monovalent cations (Na^+, K^+), it was shown that the midpoint potential of the phenoxyl/phenolate couple and

its efficiency in substrate oxidation by electron and proton transfer correlate to the Lewis acidity character of the cation [101]. In these complexes there is no correlation between the ν_{7a}(C–O) frequency or ν_{8a}(C–C)–ν_{7a}(C–O) frequency difference and the midpoint potential of the phenoxyl radical or the Lewis-acidity of the metal [101].

These data demonstrate that at least in metal-complexes, the frequencies of the ν_{7a}(C–O) and ν_{8a}(C–C) modes depend on various factors, as the nature of *ortho*- and *para*-substituents and the interactions formed by the oxygen, which are interdependent, but possibly also on other factors as the charge density of the metal, determined by the whole coordination sphere [100]. More experimental data and modelling of these various factors are needed to detail the origin of the ν_{7a}(C–O) and ν_{8a}(C–C) frequencies in these complexes.

In galactose and glyoxal oxidases, the modified cys-Tyr$^{\bullet}$ ligand of Cu has very similar ν_{8a}(C–C) and ν_{7a}(C–O) mode frequencies, at 1595–1591 and 1487–1486 cm^{-1}, although the midpoint potentials of the cys-Tyr$^{\bullet}$/cys-Tyr couples are largely different, at 640 mV for glyoxal oxidase [45] and 400 mV for galactose oxidase [111]. The frequencies of the ν_{7a}(C–O) mode of these cys-Tyr$^{\bullet}$ differ significantly from those reported for the related model compound 2,SCH_3-*para*-*tert*-phenoxyl coordinated to Cu^{2+} or Zn^{2+}, at 1512–1517 cm^{-1} [112]. These data illustrate the strong influence of the coordination sphere of the metal on the properties of the ν_{7a}(C–O) mode in these enzymes. A better knowledge of this mechanisms could unravel possible functional implications. The ν_{8a}(C–C) mode was strongly enhanced for the cys-Tyr$^{\bullet}$ ligand of Cu [45], as observed in the phenoxyl-Cu or-Fe complexes discussed above [98–100] and this is considered as a marker of metal coordination. The absence of a strong-enhanced ν_{8a}(C–C) mode in the RR spectrum of the Tyr$^{\bullet}$ of mouse ribonucleotide reductase has been taken as an evidence that this Tyr$^{\bullet}$ is not coordinated to the di-iron cluster [79].

Finally, the covalent bond between histidine and tyrosine enhances the double bond character of the tyrosinyl C–O bond. This was demonstrated by RR spectroscopy with a model of covalently bound His-Tyr, 2-imidazole-phenol. Spectra recorded with 2-imidazole-phenoxyl, unlabeled or specifically ^{18}O- and ^{2}H-labeled on the phenolic moiety, showed that the ν_{8a}(C–C) and ν_{7a}(C–O) modes of the radical appear at 1530 and 1587 cm^{-1}, respectively [113]. IR signals at 1522 or 1498 cm^{-1} have been proposed to account for the ν_{7a}(C–O) mode of the 2-imidazole-phenoxyl [95]. A signal at 1489 cm^{-1} was recently assigned by RR to the ν_{7a}(C–O) mode of the his-Tyr$^{\bullet}$ radical associated to the P-intermediate of cytochrome b_0 from *E. coli* [41]. These assignments remain, however, tentative due to the lack of experimental results with specifically labeled compounds.

5.1. Conclusions on the models

Among the reported vibrational modes of tyrosine or phenoxyl radicals, mainly the ν_{7a}(C–O) and ν_{8a}(C–C) modes are useful to diagnostic the presence and properties of Tyr$^{\bullet}$ in proteins. The intensity of the ν_{8a}(C–C) mode may reveal possible interaction of the Tyr$^{\bullet}$ with Fe or Cu. The ν_{7a}(C–O) mode detected both by IR and RR is very sensitive to the interactions formed by the Tyr$^{\bullet}$ oxygen. It is a marker of the polarity of the environment of phenoxyl radicals. Its frequency depends directly on the hydrogen bonding interactions formed by non-coordinated tyrosine radicals in proteins.

6. Tyr_Z and Tyr_D radicals in photosystem II

6.1. IR modes of $Tyr_D^{\bullet}$ and $Tyr_D^{\bullet}$ in photosystem II

PSII is not easily accessible to RR spectroscopy, due to the fluorescence from the large number of intrinsic chlorophylls. Thus, most of the vibrational data on PSII were obtained using FTIR difference spectroscopy (reviewed in Ref. [114]). The FTIR difference spectra corresponding to Tyr_D oxidation in PSII (denoted $Tyr_D^{\bullet}/Tyr_D$ spectra) have been reported on both spinach and *Synechocystis* sp. PCC 6803 PSII, using optimized experimental protocols to avoid contributions from other redox cofactors of the PSII protein, notably the quinone Q_A. Similar $Tyr_D^{\bullet}/Tyr_D$ spectra were obtained by four different research groups [81–83,115,116], while a different spectrum was reported by the research group of Prof. B.A. Barry [117–119]. Actually, a general discrepancy exists between the results of Prof. B.A. Barry and colleagues and those from the other infrared spectroscopists working on PSII, not only for spectra assigned to $Tyr_D^{\bullet}/Tyr_D$, but also for those assigned to $Tyr_Z^{\bullet}/Tyr_Z$, to oxidation of the oxygen evolving complex (S_2/S_1 spectra) and to the reduction of the primary quinone acceptor Q_A, denoted Q_A^-/Q_A [120–123]. Different independent research groups have discussed these discrepancies precisely [81,116,124].

The $Tyr_D^{\bullet}/Tyr_D$ and Q_A^-/Q_A spectra reported by us and others are illustrated in Fig. 2B and C [81–83,115,116,125–133]. These spectra are fingerprints of the changes experienced not only by the redox active species (Tyr_D and Q_A, respectively) but also by amino acid side chains and by the polypeptide backbone, influenced by the oxidoreduction reaction. Accordingly, these spectra differ largely. Tyrosine ^{13}C-labeling at the C(4) ring carbon bearing the phenolic oxygen ($^{13}C_1$(4)-Tyr) induces two clear band downshifts in the $Tyr_D^{\bullet}/Tyr_D$ spectrum (Fig. 2B) [82] that were also observed by Noguchi et al. [83], while the rest of the spectra superimpose almost perfectly. The first $Tyr_D^{\bullet}/Tyr_D$ spectra were obtained in the presence of formate in phosphate buffer pH 6 and with ferrocyanide and ferricyanide as exogenous electron donor/acceptor couple in rigorously controlled conditions to obtain solely spectral contributions from the electron donor side of PSII—i.e. $Tyr_D^{\bullet}/Tyr_D$—without contamination from the electron acceptor side, i.e. signals from Q_A^-/Q_A [81–83]. Similar spectra were then obtained in the

absence of formate and with different buffers, excluding any influence of these compounds especially on the Tyr_D and $Tyr_D^{\bullet}$ IR modes (Ref. [116] and Hienerwadel et al. in preparation).

Identical Q_A^-/Q_A spectra were reported by all research groups in the field [81,125–133]. Prof. Barry and colleagues assigned spectra similar to a Q_A^-/Q_A spectrum either to $Tyr_D^{\bullet}/Tyr_D$ or $Tyr_Z^{\bullet}/Tyr_Z$ [117–119] or to Chl^+/Chl [123]. They assigned a characteristic positive band of the Q_A^-/Q_A FTIR spectrum at 1478–1479 cm^{-1} [81,125–130] to the ν_{7a}(C–O) mode of either $Tyr_D^{\bullet}$ or $Tyr_Z^{\bullet}$ or to a mode of Chl^+[117–119,122,123]. These alternate assignments were based on the identification of spectral changes induced by specific isotope labeling or site-directed mutants in experiments which induced, however, rather intensity changes than clear band shifts [117–119]. We conclude that a mixture of IR signals from the redox tyrosines and from the acceptor quinone prevented convincing assignment of IR modes to Tyr_D, $Tyr_D^{\bullet}$, Tyr_Z, $Tyr_Z^{\bullet}$ in these spectra. These results will not be further discussed hereafter.

Due to the rapid decay of the $Tyr_Z^{\bullet}$ intermediate in oxygen evolving PSII, the IR signatures of $Tyr_Z^{\bullet}$ have been only reported in PSII samples deprived of the Mn_4Ca-cluster. Up to now, $Tyr_Z^{\bullet}/Tyr_Z$ [78] or $Tyr_Z^{\bullet}Q_A^-/Tyr_ZQ_A$ [128] FTIR difference spectra from spinach or *Synchocystis* sp. PCC 6803 have been reported.

6.1.1. ν7a(C–O) mode

In the $Tyr_Z^{\bullet}/Tyr_Z$ and $Tyr_D^{\bullet}/Tyr_D$ spectra, the IR contributions from the tyrosine itself have been deduced from comparison with model compounds [81] and by using PSII samples from *Synechocystis* sp. PCC 6803 with specifically ^{13}C- or ^{2}H-labeled tyrosine side-chains [78,82,83]. This specific labeling downshifts only the frequency of the IR modes implying motions of the labeled atoms. In particular, the use of $^{13}C_1$(4)-Tyr labeling demonstrated the contribution of the ν_{7a}(C–O) modes of $Tyr_D^{\bullet}$ at 1503 cm^{-1} and that of $Tyr_Z^{\bullet}$ at 1512 cm^{-1}. For the labeled PSII samples, these signals were unambiguously downshifted to 1476 ($Tyr_D^{\bullet}$) and 1486 cm^{-1} ($Tyr_Z^{\bullet}$) (Figs. 2B and 3) [78,82,83]. Such 27-cm^{-1} downshift upon $^{13}C_1$(4)-Tyr labeling corresponds to that observed for $Tyr^{\bullet}$ generated by UV-photochemistry in vitro (Fig. 3D, [93]). The ν_{7a}(C–O) IR mode of $Tyr_D^{\bullet}$ was observed at the same frequency, 1503 cm^{-1}, in PSII samples containing or not formate and/or phosphate buffer [81–83,115,116].

6.1.2. ν(C–C) mode

For $Tyr_Z^{\bullet}$ and $Tyr_D^{\bullet}$, another IR mode sensitive to $^{13}C_6$- and $^{2}H_4$-Tyr isotope labeling is identified at 1533–1532 cm^{-1} [78,82]. This mode, not reported by RR spectroscopy on $Tyr^{\bullet}$ models, may correspond to the IR-active ν_{19b}(C–C) mode observed at 1515 cm^{-1} for non-interacting $PhO^{\bullet}$ in an argon matrix [96]. The frequency and intensity of this IR mode may thus also be a probe of the interactions formed by $Tyr^{\bullet}$ in the protein.

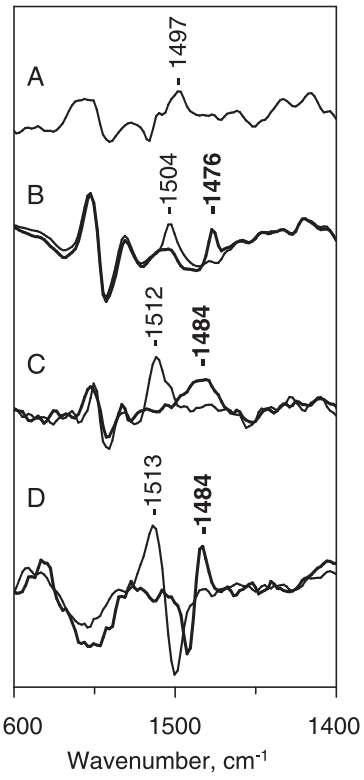

Fig. 3. FTIR difference spectra in the absorption region of ν_{7a}(C–O) IR mode of the $Tyr^{\bullet}$ radical for PSII samples from *Synechocystis* sp. PCC 6803 with unlabeled tyrosine—thin line, or $^{13}C_1$(4)-labeled tyrosine—thick line. (A) $Tyr_D^{\bullet}/Tyr_D$ in the D2His189Gln mutant [59], (B) $Tyr_D^{\bullet}/Tyr_D$ in WT [59], (C) $Tyr_Z^{\bullet}/Tyr_Z$ in WT PSII [54]. (D) $Tyr^{\bullet}/Tyr^-$ recorded with 10 mM ^{12}C- (thin line) or $^{13}C_1$(4)- (thick line) tyrosinate solutions in borate buffer pH 12 [72].

6.2. Effect of hydrogen-bonding interaction on the ν_{7a}(C–O) IR mode

The hydrogen bond formed by $Tyr_D^{\bullet}$ to D2His189 is disrupted in the D2His189Gln mutant of *Synechocystis* sp. PCC 6803 [71]. $Tyr_D^{\bullet}/Tyr_D$ FTIR difference spectra recorded with this D2His189Gln mutant with unlabeled or $^{2}H_4$-labeled Tyr demonstrated that the ν_{7a}(C–O) mode of $Tyr_D^{\bullet}$ in this mutant contributes at 1498 cm^{-1} (Fig. 3, Ref. [82]). Therefore, it was concluded that the hydrogen bond formed between D2His189 and $Tyr_D^{\bullet}$ induced an up-shift by 6 cm^{-1} of the $Tyr_D^{\bullet}$ ν_{7a}(C–O) mode [82].

The ν_{7a}(C–O) mode of $Tyr_Z^{\bullet}$ at 1512 cm^{-1} thus indicates that $Tyr_Z^{\bullet}$ is more strongly hydrogen-bonded than $Tyr_D^{\bullet}$ in Mn-depleted PSII [82]. It was proposed that $Tyr_Z^{\bullet}$ forms a strong hydrogen bond to D1His190, the histidine homologous to D2His189 on the D1 polypeptide. This residue has been proposed at hydrogen bonding distance from Tyr_Z in the recent three dimensional structure of PSII [18]. Alternately, additional hydrogen bonding to another base could explain the ν_{7a}(C–O) mode frequency. In particular, the frequency observed for $Tyr_Z^{\bullet}$ coincides with that obtained for $Tyr^{\bullet}$ formed by UV-photochemistry in frozen borate buffer,

where Tyr• is hydrogen-bonded to water molecules (Fig. 3). The IR mode of $Tyr_Z^{\bullet}$ at 1512 cm^{-1} has a larger width at half height (13 cm^{-1}) than that of $Tyr_D^{\bullet}$ (9 cm^{-1}). The same feature is found for the $^{13}C_1(4)$-labeled ν_{7a}(C−O) at 1484 and 1476 cm^{-1}(Fig. 3). This may correspond to the more distributed hydrogen bonding pattern of Tyr• deduced from the ^{2}H-ESE-ENDOR analysis [134].

The ν_{7a}(C−O) mode of the non-hydrogen-bonded Tyr• from *E. coli* ribonucleotide reductase is reported at 1498 cm^{-1} [2]. The same ν_{7a}(C−O) mode frequency is observed in PSII for the non-hydrogen-bonded $Tyr_D^{\bullet}$ in the D2His189Gln mutant. This ν_{7a}(C−O) mode was recently identified at 1515 cm^{-1} for the Tyr• in the ribonucleotide reductase from mouse [79]. In this enzyme, hydrogen bonding between the Tyr• and a water molecule ligand of the iron was deduced from the 5-cm^{-1} downshift observed for the ν_{7a}(C−O) mode upon H/^{2}H exchange [79] and from the Tyr• HF-EPR spectrum [135] (see below). These data, together with the frequency of the ν_{7a}(C−O) mode reported at 1481 cm^{-1} for the phenoxyl radical obtained in argon matrix, i.e. free from interactions [96], are fully consistent with the observation that the formation of a hydrogen bond will significantly increase the ν_{7a}(C−O) mode frequency of Tyr• in proteins. The relationship between the ν_{7a}(C−O) mode frequency and the type of hydrogen bonding interaction should be now analyzed into details to probe the environment of radicals in proteins. In particular, the effect of a charge on the interacting group on the IR frequency should be determined.

6.2.1. Theoretical calculations—hydrogen bonding interactions

The normal modes of the radicals phenoxyl, *p*-methyl-phenoxyl and Tyr• have been determined using DFT calculation techniques to model the structure of the tyrosine radicals [90,108–110,136,137]. These calculations also reside on the reproduction of the spin densities and hyperfine couplings determined experimentally by EPR spectroscopy [109,138,139]. A hydrogen bonding interaction between the phenoxyl radical and two water molecules induces an upshift of the ν_{7a}(C−O) mode of the phenoxyl radical by ≈ 29 cm^{-1} [110]. Positive charges near the phenoxyl oxygen also induce an upshift of the ν_{7a}(C−O) mode [137]. For *p*-methyl-phenoxyl hydrogen-bonded to imidazole, the ν_{7a}(C−O) mode frequency also depends on the charge density residing on the imidazole moiety [137]. It is upshifted by 22 cm^{-1} upon hydrogen bonding to an imidazolium as compared to a neutral imidazole [137]. Intermediary frequencies are computed, if a charge at larger distance from the radical is localized on a base hydrogen-bonded to the imidazole [137]. From these theoretical studies and for a model where both Tyr_D an Tyr_Z are hydrogen-bonded to the imidazole side chain of a histidine, the lower frequency observed for the ν_{7a}(C−O) mode of $Tyr_D^{\bullet}$ compared to $Tyr_Z^{\bullet}$ could result from a larger proton delocalization upon $Tyr_D^{\bullet}$ formation, through amino acids hydrogen-bonded to the histidine. Differences between $Tyr_Z^{\bullet}$ and $Tyr_D^{\bullet}$ due to (an additional) hydrogen bond between $Tyr_Z^{\bullet}$ and a water molecule, however, cannot be excluded at present.

Another theoretical simulation suggested a non-monotonic behavior of the frequency of the ν_{7a} (C−O) mode as a function of the distance between the phenoxyl oxygen and a hydrogen-bonded water molecule [80]. A slight upshift of the ν_{7a}(C−O) mode is calculated upon hydrogen bonding to one or two water molecules for O∘∘∘H distances greater than 1.65 Å, while for shorter distances, the ν_{7a}(C−O) mode shifts down rapidly. This is explained by a less stable structure, due to repulsive coulombic interaction between the phenoxyl ring and the hydrogen atom [80]. These data would rationalize the rather low frequency assigned to the ν_{7a}(C−O) mode of the Tyr• by RR in bovine liver catalase, 1488–1484 cm^{-1}, depending on pH [80], as compared to the other frequencies reported for Tyr• in proteins (1497–1515 cm^{-1}, Table 1). The unambiguous assignment of Tyr• contribution at 1488–1484 cm^{-1} in this study, however, awaits experiments performed with specifically labeled tyrosines. The tyrosine implicated in radical formation is not identified, but the hydrogen bond between this Tyr• and its environment was deduced from its HF-EPR spectrum [80].

6.2.2. Comparison of vibrational data and HF-EPR and ESEEM-ENDOR data

HF-EPR data are available for Tyr• obtained in amino-Tyr or HCl-Tyr crystals irradiated with γ rays [28,140,141] and for the Tyr• of *E. coli* or mouse ribonucleotide reductase and of PSII. These data showed that the anisotropy of the *g*-factor, as well as the value of the g_x tensor oriented along the Tyr• C−O axis, depend on electrostatic interactions formed by the radical and its environment [80,135,142–145]. The g_x values of the radicals are presented in Table 2. They are paralleled with the ν_{7a}(C−O) mode frequency determined by IR or RR spectroscopy and with the information on hydrogen-bonding pattern of the radical deduced from the crystallographic structure or from ENDOR or ESEEM data. This table shows that electrostatic and/or hydrogen bonding interactions induce an upshift of the Tyr• ν_{7a}(C−O) mode that roughly correlates with decreasing values of the g_x tensor. The only exception is for the Tyr• observed in beef liver catalase. Both HF-EPR and IR data recorded on Tyr• in non-hydrogen-bonded, non-charged environment (1481 cm^{-1} and 2.0094, respectively) reinforce this correlation. To confirm these correlations, RR data on Tyr• in γ-irradiated Tyr-HCl crystals would be necessary as well as isotope labeling experiments on beef liver catalase, to definitely assign the ν_{7a}(C−O) mode of the Tyr• radical, which largely differs from the other data.

For $Tyr_D^{\bullet}$ and $Tyr_Z^{\bullet}$, similar g_x values are detected by HF-EPR, and similar hydrogen-bonding strength deduced from

Table 2
Summary of data obtained by FTIR/RR, HF-EPR and ENDOR/ESSEM/X-ray spectroscopies on $Tyr^{\bullet}$ or *p*-methyl-phenoxyl radicals

Radical	IR or RR (cm^{-1})	HF-EPR (*g* value)	Interactions, proposed according to ENDOR or ESEEM or X-ray structure
Phenoxyl (Argon)	1481[a]	–	no interactions, no charges
N-Acetyl-$Tyr^{\bullet}$		2.0094[b]	no interactions, no charges
E. coli class I RR	1498[c]	2.0089[d]	electrostatic interaction with Fe_2 (dist. 5.4 Å) no hydrogen bond[e,f]
$Tyr^{\bullet}$		2.0091[g]	
Salmonella typhimurium		2.0090[h]	
PS II D2His189Gln	1497[i]	2.0083[j]	No hydrogen bond[k]
PS II $Tyr_D^{\bullet}$	1503[i,l]	2.0074[j]	1 or 2 ∘∘∘H, 1.67 Å or 1.87 Å (depending on organism)[m]
Spinach	1505		
PS II $Tyr_Z^{\bullet}$	1512[n]	2.0075[j]	∘∘∘H disordered, average dist. 1.95 Å[m]
Mouse RR $Tyr^{\bullet}$	1515[o]		∘∘∘H 1.89 Å[f] likely water ligand at Fe_1
	(1510 in ^2H_2O)		
Herpes simplex virus		2.0076[p] (large splitting)	∘∘∘H 1.86 Å[f]
$Tyr^{\bullet}-H_2O$	1515[qr]		∘∘∘H and/or interactions with Na^+
$Tyr^{\bullet}$ –HCl crystal	–	2.0067[s]	1.6 Å dist. to COOH
		2.00[t]	3 Å dist. to Cl^-
Catalase $Tyr^{\bullet}$	1484[u]	2.0073[u] (2.0065 minor fraction)	hypothesis of a ∘∘∘H with distance < 1.65 Å

[a] Spanget-Larsen et al. [96]. [b] Mezetti et al. [140]. [c] Backes et al. [2]. [d] Un et al. [143]. [e] Hoganson et al. [149]. [f] van Dam et al. [150]. [g] Himo et al. [138]. [h] Allard et al. [148]. [i] Hienerwadel et al. [82]. [j] Un et al. [144]. [k] Tang et al. [71]. [l] Noguchi et al. [83]. [m] Force et al. [134]. [n] Berthomieu et al. [78]. [o] Hanson et al. [79]. [p] Schmidt et al. [135]. [q] Tripathi and Schuler [85]. [r] Berthomieu et al. [93]. [s] Fasanella and Gordy [141]. [t] Ivancich et al. [28]. [u] Ivancich et al. [80].

the ^{2}H-ESE-ENDOR experiments [134]. The broad signals observed both in HF-EPR and ENDOR for $Tyr_Z^{\bullet}$ were interpreted as a distribution of slightly different hydrogen bonds. The frequency difference between the ν_{7a}(C−O) IR mode of $Tyr_Z^{\bullet}$ and $Tyr_D^{\bullet}$ may result from these different populations or from chemically different hydrogen bonding partners. HF-EPR, ENDOR, ESEEM and vibrational spectroscopies are complementary to describe the interactions formed by a radical and its environment. Additional RR and IR data on radicals with known hydrogen-bonding partners will contribute to precise the correlation existing between the spectroscopic data, the radical structures and the interactions performed with the environment.

7. pK_A of Tyr_D and Tyr_Z and proton transfer reactions following radical formation

The pH and temperature dependences of the reduction kinetics of P_{680}^+ by Tyr_D or Tyr_Z in Mn-depleted PSII point to proton-concerted electron transfer mechanisms, with apparent pK_A of 7.5–7.7 for Tyr_D to P_{680}^+ [73–75], and pK_A(s) ranging form 5.5 to 10 for Tyr_Z to P_{680}^+ [12,13,65–67]. Whether these pK_As correspond to Tyr_D, Tyr_Z, to the nearby histidine (distal nitrogen) D2His189 and D1His190, or to an apparent pK_A resulting from changes within a larger number of interacting groups, can be analyzed by FTIR spectroscopy.

Specific infrared (and RR) modes can be used to discriminate neutral tyrosine (TyrOH) from tyrosinate. The ν_{19}(C−C) contributes at ≈ 1518 cm^{-1} for TyrOH and at ≈ 1500 cm^{-1} for tyrosinate (Refs. [82,83] and references therein). The intense tyrosinate ν_{19}(C−C) mode is clearly observed in UV-induced $Tyr^{\bullet}/Tyr^-$FTIR spectra (Fig. 3) [92–94]. This signal is absent in the $Tyr_D^{\bullet}/Tyr_D$ and $Tyr_Z^{\bullet}/Tyr_Z$ FTIR difference spectra, while signals at 1513–1510 cm^{-1} for Tyr_D, and at 1521 cm^{-1} for Tyr_Z, sensitive to Tyr $^{13}C_1$(4), $^2H_4$, and $^{13}C_6$-Tyr labeling, were assigned to this ν_{19}(C−C) mode, with frequencies showing that Tyr_D and Tyr_Z are neutral TyrOH at pH 6 [78,82,83].

In the IR domain where the ν(C−O) or/and δ(COH) modes of reduced tyrosinate or tyrosine are expected to contribute (1300–1100 cm^{-1}), two IR modes have been unambiguously identified for Tyr_D and Tyr_Z using $^{13}C_1$(4)-labeling [78,82]. For the model compound, *p*-methyl-phenol, the frequency and intensity of the two IR active modes ν(C−O) and δ(COH) in this region are sensitive to the presence and strength of an hydrogen bond and to the nature of the hydrogen-bonded chemical group, hydroxyl, carbonyl, pyridine nitrogen, imidazole (ImH) or imidazolium (ImH_2^+) [82]. The ν(C−O) and δ(COH) IR frequencies identified for Tyr_D at 1275 and 1250 cm^{-1} and for Tyr_Z at 1279 and 1255 cm^{-1}, respectively, correspond at best with a model where both Tyr_D and Tyr_Z are protonated at pH 6 and hydrogen-bonded to the neutral side chain of a histidine in PSII. Noguchi et al. [83] also assigned the signal at 1256 cm^{-1} to neutral Tyr_D by comparison with the IR spectrum of TyrOH. Recently, normal mode calculations using density functional theory on *p*-methyl-phenol-imidazole complexes reproduced the experimental IR data, in favor of the hydrogen bond between protonated Tyr_D or Tyr_Z and the neutral side-chain of a histidine [137].

For Tyr_D, these IR data are in agreement with the general view that Tyr_D and $Tyr_D^{\bullet}$ both interact with D2His189, and that radical formation leads to proton transfer to the nearby histidine. The slightly higher frequency observed for the δ(COH) mode of Tyr_Z as compared to Tyr_D may indicate a stronger interaction with its environment or a more electronegative environment than for Tyr_D. These IR data, how-

ever, are in favor of a hydrogen bond between reduced Tyr_Z and D1His190. A weakening or disruption of the Tyr_Z–D1His190 hydrogen bond interaction upon Tyr_Z oxidation could explain both the IR and kinetic or ^{15}N ESE-ENDOR data [12,66].

For oxygen evolving PSII, contradictory results are proposed concerning the protonation of reduced Tyr_Z and its pK_A [83] (reviewed in Ref. [63]). Noguchi et al. [83] assigned two IR modes at 1522 and 1254 cm^{-1} to Tyr_Z in the FTIR difference spectrum corresponding to the S_1-to-S_2 transition in *Synechocystis* sp. PCC 6803. These frequencies are similar to those identified for Tyr_Z in Mn-depleted PSII [78]. If the Tyr signals identified unambiguously using PSII samples with $^{13}C_1(4)$-labeled tyrosines are due to Tyr_Z (and not Tyr_D), they provide experimental evidence that Tyr_Z is protonated in oxygen evolving PSII and forms hydrogen bonding interactions equivalent to those in Mn-depleted PSII. Upon S_1-to-S_2 transition, the Tyr IR modes experience an intensity decrease without changes in frequency. Thus, the oxidation of the Mn cluster does not modify the hydrogen-bonding interactions formed by Tyr_Z, in disagreement with a direct connection between Tyr_Z and the oxidized Mn site in the Mn_4 cluster. The band at 1254 cm^{-1} is not present in the S2/S1 spectrum recorded with spinach PSII [83,146,147] while two IR modes at 1522 and 1246 cm^{-1}, sensitive to Ca^{2+} depletion, have been assigned to Tyr_Z and taken as indication that Ca^{2+} depletion perturbs the hydrogen bonding network around Tyr_Z [146]. The origin of the 1522, 1256 and 1244–1246 cm^{-1} bands should be confirmed in these S2/S1 spectra, to better understand the interactions existing between Tyr_Z, Ca^{2+} and Mn.

Knowing that Tyr_D and Tyr_Z are protonated at pH 6 in Mn-depleted PSII, the proton accepting group(s) upon $Tyr_D^{\bullet}$ and $Tyr_Z^{\bullet}$ formation should be precised. For Tyr_D, a proton shuttling model is proposed between D2His189 and Tyr_D, while for Tyr_Z, it was proposed that D1His190 and D1Glu189 are involved in a proton transfer pathway. $Tyr_D^{\bullet}/Tyr_D$ spectra recorded on PSII centers with ^{13}C-labeled histidine in phosphate buffer at pH 6 in the presence of formate, however, did not evidence the IR ν(C–C) mode of histidinium ($HisH_2^+$) expected to induce a small isotope-sensitive signal around 1633 cm^{-1} [82]. In contrast, positive IR bands between 1700 and 1740 cm^{-1} in the $Tyr_D^{\bullet}/Tyr_D$ spectrum suggested that aspartic or glutamic groups protonate during radical formation. The FTIR data also show that proton uptake by the phosphate buffer accompanies $Tyr_D^{\bullet}$ formation in these samples. These IR data suggest that the apparent pK_A determined from the pH dependence of the reduction kinetic of P_{680}^+ by Tyr_D in Tyr_Z-less mutants [74] could correspond to proton transfer from Tyr_D to HisD2-189, in which the distal His proton has to leave. There is no equivalent of these signals in the $Tyr_Z^{\bullet}/Tyr_Z$ FTIR difference spectrum [78]. Experiments as a function of pH are underway to determine the pK_A of Tyr_D, Tyr_Z, and neighbouring histidines.

8. Conclusions

Infrared and RR spectroscopies can provide key information relative to the properties of tyrosine radicals in proteins as well as to the role of tyrosine radicals in electron transfer and hydrogen abstraction reactions. This role can be deduced from specific interactions of the tyrosine with its protein environment. For PSII, infrared marker signals of tyrosine for both the reduced and radical state have been identified, which precise the protonation state and specific hydrogen bonding interaction of the tyrosines Tyr_D and Tyr_Z with their environment. The development of adapted kinetic setups in the mid-infrared domain should bring the time resolution (ns) necessary to identify the characteristic tyrosine IR modes in intact PSII and the amino acids involved in proton transfer reactions upon water oxidation.

Acknowledgements

We acknowledge the contributions of Drs. Alain Boussac, Jacques Breton, Bruce Diner and Eliane Nabedryk to the FTIR work described here. We also acknowledge fruitful discussions with Dr. Warwick Hillier, Prof. Richard Debus, and Prof. Takumi Noguchi.

References

[1] J. Stubbe, W.A. van der Donk, Protein Radicals in Enzyme Catalysis, Chem. Rev. 98 (1998) 705–762 and 2661–2662.
[2] G. Backes, M. Sahlin, B.-M. Sjöberg, T.M. Loehr, J. Sanders-Loehr, Resonance Raman spectroscopy of ribonucleotide reductase. Evidence for a deprotonated tyrosyl radical and photochemistry of the binuclear iron center, Biochemistry 28 (1989) 1923–1929.
[3] J.R. Bollinger, D.E. Edmondson, B.H. Huynh, J. Filley, J.R. Norton, J. Stubbe, Mechanism of assembly of the tyrosyl radical-dinuclear iron cluster cofactor of ribonucleotide reductase, Science 253 (1990) 292–298.
[4] B.A. Barry, G.T. Babcock, Tyrosine radicals are involved in the photosynthetic oxygen-evolving system, Proc. Natl. Acad. Sci. U. S. A. 84 (1987) 7099–7103.
[5] B.A. Barry, M.K. El-Deeb, P.O. Sandusky, G.T. Babcock, Tyrosine radicals in photosystem II and related model compounds. Characterization by isotopic labeling and EPR spectroscopy, J. Biol. Chem. 265 (1990) 20139–20143.
[6] M. Högbom, M. Galander, M. Andersson, M. Kolberg, W. Hofbauer, G. Lassmann, P. Nordlund, F. Lendzian, Displacement of the tyrosyl radical cofactor in ribonucleotide reductase obtained by single-crystal high-field EPR and 1.4-Å X-ray data, Proc. Natl. Acad. Sci. U. S. A. 100 (2003) 3209–3214.
[7] J. Stubbe, Di-iron-tyrosyl radical ribonucleotide reductases, Curr. Opin. Chem. Biol. 7 (2003) 183–188.
[8] D.J. Silva, J. Stubbe, V. Samano, M.J. Robins, Gemcitabine 5′-triphosphate is a stoichiometric mechanism-based inhibitor of *Lactobacillus leichmannii* ribonucleoside triphosphate reductase: evidence for thiyl radical-mediated nucleotide radical formation, Biochemistry 37 (1998) 5528–5535.
[9] J. Stubbe, P. Riggs-Gelasco, Harnessing free radicals: formation and function of the tyrosyl radical in ribonucleotide reductase, TIBS 23 (1998) 438–443.
[10] H. Eklund, M. Eriksson, U. Uhlin, P. Nordlund, D. Logan, Ribonu-

cleotide reductase—structural studies of a radical enzyme, J. Biol. Chem. 378 (1997) 821–825.
[11] B.A. Diner, G.T. Babcock, Structure, dynamics, and energy conversion efficiency in photosystem II, in: D.R. Ort, C.F. Yocum (Eds.), Oxygenic Photosynthesis: The Light Reactions, Kluwer Academic Publishing, Boston, MA, 1996, pp. 213–247.
[12] B.A. Diner, Amino acid residues involved in the coordination and assembly of the manganese cluster of photosystem II. Proton-coupled electron transport of the redox-active tyrosines and its relationship to water oxidation, Biochim. Biophys. Acta 1503 (2001) 147–163.
[13] R.J. Debus, Amino acid residues that modulate the properties of tyrosine Y(Z) and the manganese cluster in the water oxidizing complex of photosystem II, Biochim. Biophys. Acta 1503 (2001) 164–186.
[14] M.L. Gilchrist, J.A. Ball, D.W. Randall, R.D. Britt, Proximity of the manganese cluster of photosystem II to the redox-active tyrosine YZ, Proc. Natl. Acad. Sci. U. S. A. 92 (1995) 9545–9549.
[15] R.D. Britt, Oxygen evolution, in: C.Y. Yocum, D. Ort (Eds.), Advances in Photosynthesis: Oxygenic Photosynthesis, The Light Reactions, Kluwer Academic Publishing, Dordrecht, The Netherlands, 1996, pp. 137–164.
[16] A. Zouni, H.T. Witt, J. Kern, P. Fromme, N. Krauss, W. Saenger, P. Orth, Crystal structure of photosystem II from *Synechococcus elongatus* at 3.8 A resolution, Nature 409 (2001) 739–743.
[17] N. Kamiya, J.R. Shen, Crystal structure of oxygen-evolving photosystem II from *Thermosynechococcus vulcanus* at 3.7-A resolution, Proc. Natl. Acad. Sci. U. S. A. 100 (2003) 98–103.
[18] K.N. Ferreira, T.M. Iverson, K. Maghlaoui, J. Barber, S. Iwata, Architecture of the photosynthetic oxygen-evolving center, Science 303 (2004) 1831–1838.
[19] A.W. Rutherford, A. Boussac, P. Faller, The stable tyrosyl radical in photosystem II: why D? Biochim. Biophys. Acta. 1655 (2004) 222–230.
[20] R. Karthein, R. Dietz, W. Nastainczyk, H.H. Ruf, Higher oxidation states of prostaglandin H synthase. EPR study of a transient tyrosyl radical in the enzyme during the peroxidase reaction, Eur. J. Biochem. 171 (1988) 313–320.
[21] A.-L. Tsai, L.C. His, R.J. Kulmacz, G. Palmer, W.L. Smith, Characterization of the tyrosyl radicals in bovine prostaglandin H synthase-1 by isotope replacement and site-directed mutagenesis, J. Biol. Chem. 269 (1994) 5085–5091.
[22] A. Tsai, R.J. Kulmacz, G. Palmer, Spectroscopic evidence for reaction of prostaglandin H synthase-1 tyrosyl radical with arachidonic acid, J. Biol. Chem. 270 (1995) 10503–10508.
[23] A. Tsai, G. Wu, G. Palmer, B. Bambai, J.A. Koehni, P.J. Marshalli, R.J. Kulmacz, Rapid kinetics of tyrosyl radical formation and heme redox state changes in Prostaglandin H synthase-1 and -2, J. Biol. Chem. 274 (1999) 21695–21700.
[24] M.G. Malkowski, S.L. Ginell, W.L. Smith, R.M. Garavito, The productive conformation of arachidonic acid bound to prostaglandin synthase, Science 289 (2000) 1933–1937.
[25] B.H. Dunford, Heme Peroxidases, Wiley, New York, 1999.
[26] M. Sivaraja, D.B. Goodin, M. Smith, B. Hoffman, Identification by ENDOR of Trp191 as the free-radical site in cytochrome *c* peroxidase compound ES, Science 245 (1989) 738–740.
[27] A. Ivancich, H.-M. Jouve, B. Sartor, J. Gaillard, EPR investigation of compound I in *Proteus mirabilis* and bovine liver catalases: formation of porphyrin and tyrosyl radical intermediates, Biochemistry 36 (1997) 9356–9364.
[28] A. Ivancich, P. Dorlet, D.B. Goodin, S. Un, Multifrequency high-field EPR study of the tryptophanyl and tyrosyl radical intermediates in wild-type and the W191G mutant of cytochrome *c* peroxidase, J. Am. Chem. Soc. 123 (2001) 5050–5058.
[29] A. Ivancich, G. Mazza, A. Desbois, Comparative electron paramagnetic resonance study of radical intermediates in turnip peroxidase isozymes, Biochemistry 40 (2001) 6860–6866.
[30] S. Chouchane, S. Girotto, S. Yu, R.S. Magliozzo, Identification and characterization of tyrosyl radical formation in *Mycobacterium tuberculosis* catalase-peroxidase (KatG), J. Biol. Chem. 277 (2002) 42633–42638.
[31] A. Ivancich, C. Jakopitsch, M. Auer, S. Un, C. Obinger, Protein-based radicals in the catalase-peroxidase of *Synechocystis* PCC6803: a multifrequency EPR investigation of wild-type and variants on the environment of the heme active site, J. Am. Chem. Soc. 125 (2003) 14093–14102.
[32] C. Aubert, P. Mathis, A.P. Eker, K. Brettel, Intraprotein electron transfer between tyrosine and tryptophan in DNA photolyase from *Anacystis nidulans*, Proc. Natl. Acad. Sci. U. S. A. 96 (1999) 5423–5427.
[33] C. Aubert, M.H. Vos, P. Mathis, A.P. Eker, K. Brettel, Intraprotein radical transfer during photoactivation of DNA photolyase, Nature 405 (2000) 586–590.
[34] B. Giovani, M. Byrdin, M. Ahmad, K. Brettel, Light-induced electron transfer in a cryptochrome blue-light photoreceptor, Nat. Struct. Biol., 10 (2004) 489–490.
[35] C. Ostermeier, A. Harrenga, U. Ermler, H. Michel, Structure at 2.7 A resolution of the *Paracoccus denitrificans* two-subunit cytochrome *c* oxidase complexed with an antibody FV fragment, Proc. Natl. Acad. Sci. U. S. A. 94 (1997) 10547–10553.
[36] S. Yoshikawa, K. Shinzawa-Itoh, R. Nakashima, R. Yaono, E. Yamashita, N. Inoue, M. Yao, M.J. Fei, C.P. Libeu, T. Mizushima, H. Yamaguchi, T. Tomozaki, T. Tsukihara, Redox-coupled crystal structural changes in bovine heart cytochrome *c* oxidase, Science 280 (1998) 1723–1729.
[37] S. Iwata, C. Ostermeier, B. Ludwig, H. Michel, Structure at 2.8 A resolution of cytochrome *c* oxidase from *Paracoccus denitrificans*, Nature 376 (1995) 660–669.
[38] T. Tsukihara, H. Aoyama, E. Yamashita, T. Tomizaki, H. Yamaguchi, K. Shinzawa-Itoh, R. Nakashima, R. Yaono, S. Yoshikawa, Structures of metal sites of oxidized bovine heart cytochrome *c* oxidase at 2.8 A, Science 269 (1995) 1069–1074.
[39] D.A. Proshlyakov, M.A. Pressler, C. DeMaso, J.F. Leykam, D.L. DeWitt, G.T. Babcock, Oxygen activation in respiration: involvement of redox-active tyrosine 244, Science 290 (2000) 1588–1591.
[40] F. MacMillan, A. Kannt, J. Behr, T. Prisner, H. Michel, Direct evidence for a tyrosine radical in the reaction of cytochrome *c* oxidase with hydrogen peroxide, Biochemistry 38 (1999) 9179–9184.
[41] T. Uchida, T. Mogi, T. Kitagawa, Resonance Raman studies of oxo intermediates in the reaction of pulsed cytochrome b_0 with hydrogen peroxide, Biochemistry 39 (2000) 6669–6678.
[42] M.M. Whittaker, J.M. Whittaker, A tyrosine-derived free radical in apogalactose oxidase, J. Biol. Chem. 265 (1990) 9610–9613.
[43] G.T. Babcock, M.K. El-Deeb, P.O. Sandusky, M.M. Whittaker, J.W. Whittaker, Electron paramagnetic resonance and electron nuclear double resonance spectroscopies of the radical site in galactose oxidase and of thioether-substituted phenol model compounds, J. Am. Chem. Soc. 114 (1992) 3727–3734.
[44] M.M. Whittaker, Y.Y. Chuang, J.W. Whittaker, Models for the redox active site in galactose oxidase, J. Am. Chem. Soc. 115 (1993) 10029–10035.
[45] M.M. Whittaker, P.J. Kersten, N. Nakamura, J. Sanders-Loehr, E.S. Schweizer, J.W. Whittaker, Glyoxal oxidase from *Phanerochaete chrysosporium* is a new radical-copper oxidase, J. Biol. Chem. 271 (1996) 681–687.
[46] N. Ito, S.E.V. Phillips, C. Stevens, Z.B. Ogel, M.J. McPherson, J.N. Keen, K.D.S. Yadav, P.F. Knowles, Novel thioether bond revealed by a 1.7 A crystal structure of galactose oxidase, Nature 350 (1991) 87–90.
[47] J.W. Whittaker, Free radical catalysis by galactose oxidase, Chem. Rev. 103 (2003) 2347–2363.
[48] R. Matsuzaki, T. Fukui, H. Sato, Y. Ozaki, K. Tanizawa, Generation of the topa quinone cofactor in bacterial monoamine oxidase by cupric ion-dependent autooxidation of a specific tyrosyl residue, FEBS Lett. 351 (1994) 360–364.

[49] D. Cai, J.P. Klinman, Copper amine oxidase: heterologous expression, purification, and characterization of an active enzyme in *Saccharomyces cerevisiae*, Biochemistry 33 (1994) 337647–337653.
[50] G.J. Gerfen, W.A. van der Donk, G. Yu, J.R. McCarthy, E.T. Jarvi, D.P. Matthews, C. Farrar, R.G. Griffin, J. Stubbe, Characterization of a substrate-derived radical detected during the inactivation of ribonucleotide reductase from Escherichia coli by 2′-fluoromethylene-2′-deoxycytidine 5′-diphosphate, J. Am. Chem. Soc. 120 (1998) 3823–3835.
[51] J. Coves, L. Le Hir de Fallois, L. Le Pape, J.L. Decout, M. Fontecave, Inactivation of Escherichia coli ribonucleotide reductase by 2′-deoxy-2′-mercaptouridine 5′-diphosphate. Electron paramagnetic resonance evidence for a transient protein perthiyl radical, Biochemistry 35 (1996) 8595–8602.
[52] M.M. Whittaker, J. Whittaker, Catalytic Reaction profile for alcohol oxidation by galactose oxidase, Biochemistry 40 (2001) 7140–7148.
[53] G.T. Babcock, The oxygen-evolving complex in photosystem II as a metallo-radical enzyme, in: P. Mathis (Ed.), Photosynthesis: From Light to Biosphere, vol II. Kluwer Acad. Pub., Dordrecht, 1995, pp. 209–215.
[54] X.S. Tang, M. Zheng, D.A. Chisholm, G.C. Dismukes, B.A. Diner, Investigation of the differences in the local protein environments surrounding tyrosine radicals $Y_Z^{\bullet}$ and $Y_D^{\bullet}$ in photosystem II using wild-type and the D2-Tyr160Phe mutant of *Synechocystis* 6803, Biochemistry 35 (1996) 1475–1484.
[55] C. Tommos, G.T. Babcock, Oxygen production in nature: a light-driven metalloradical enzyme process, Acc. Chem. Res. 31 (1998) 18–25.
[56] J.S. Vrettos, J. Limburg, G.W. Brudvig, Mechanism of photosynthetic water oxidation: combining biophysical studies of photosystem II with inorganic model chemistry, Biochim. Biophys. Acta 1503 (2001) 229–245.
[57] R.J. Debus, The manganese and calcium ions of photosynthetic oxygen evolution, Biochim. Biophys. Acta 1102 (1992) 269–352.
[58] V.K. Yachandra, K. Sauer, M.P. Klein, Manganese cluster in photosynthesis: where plants oxidize water to dioxygen, Chem. Rev. 96 (1996) 2927–2950.
[59] J. Messinger, Towards understanding the chemistry of photosynthetic oxygen evolution: dynamic structural changes, redox states and substrate water binding of the Mn cluster in photosystem II, Biochim. Biophys. Acta 1459 (2000) 481–488.
[60] C.W. Hoganson, N. Lydakis-Simantiris, X.-S. Tang, C. Tommos, K. Wranke, G.T. Babcock, B.A. Diner, J. McCraken, S. Styring, A hydrogen-atom abstraction model for the function of YZ. in photosynthetic oxygen evolution, Photosynth. Res. 46 (1995) 177–184.
[61] M. Haumann, W. Junge, The rates of proton uptake and electron transfer at the reducing side of photosystem II in thylakoids, FEBS Lett. 347 (1994) 45–50.
[62] E. Schlodder, H.T. Witt, Stoichiometry of proton release from the catalytic center in photosynthetic water oxidation. Reexamination by a glass electrode study at pH 5.5–7.2, J. Biol. Chem. 274 (1999) 30387–30392.
[63] F. Rappaport, J. Lavergne, Coupling of electron and proton transfer in the photosynthetic water oxidase, Biochim. Biophys. Acta 1503 (2001) 246–259.
[64] B.A. Diner, E. Schlodder, P.J. Nixon, W.J. Coleman, F. Rappaport, J. Wermaas, W.F.J. Wermaas, D.A. Chisholm, Site-directed mutations at D1-His198 and D2-His197 of photosystem II in *Synechocystis* PCC 6803: sites of primary charge separation and cation and triplet stabilization, Biochemistry 40 (2001) 9265–9281.
[65] B.A. Diner, D.A. Force, D.W. Randall, R.D. Britt, Hydrogen bonding, solvent exchange, and coupled proton and electron transfer in the oxidation and reduction of redox-active tyrosine YZ in Mn-depleted core complexes of photosystem II, Biochemistry 37 (1998) 17931–17943.
[66] A.M. Hays, I.R. Vassiliev, J.H. Golbeck, R.J. Debus, Role of D1-His190 in the proton-coupled oxidation of tyrosine YZ in manganese-depleted photosystem II, Biochemistry 37 (1999) 11851–11865.
[67] R. Ahlbrink, M. Haumann, D. Cherepanov, O. Bogershausen, A. Mulkidjanian, W. Junge, Function of tyrosine Z in water oxidation by photosystem II: electrostatical promotor instead of hydrogen abstractor, Biochemistry 37 (1998) 1131–1142.
[68] M. Karge, K.D. Irrgang, S. Sellin, R. Feinaugle, B. Liu, H.J. Eckert, H.J. Eichler, G. Renger, Effects of hydrogen/deuterium exchange on photosynthetic water cleavage in PSII core complexes from spinach, FEBS Lett. 378 (1996) 140–144.
[69] K.A. Campbell, J.M. Peloquin, B.A. Diner, X.-S. Tang, D.A. Chisholm, R.D. Britt, The tau-Nitrogen of D2 Histidine 189 is the Hydrogen Bond Donor to the Tyrosine Radical YD of Photosystem II, J. Am. Chem. Soc. 119 (1997) 4787–4788.
[70] B. Svensson, I. Vass, E. Cedergren, S. Styring, Structure of donor side components in photosystem II predicted by computer modelling, EMBO J. 9 (1990) 2051–20599.
[71] X.S. Tang, D.A. Chisholm, G.C. Dismukes, G.W. Brudvig, B.A. Diner, Spectroscopic evidence from site-directed mutants of *Synechocystis* PCC6803 in favor of a close interaction between histidine 189 and redox-active tyrosine 160, both of polypeptide D2 of the photosystem II reaction center, Biochemistry 32 (1993) 13742–13748.
[72] C. Tommos, L. Davidsson, B. Svensson, C. Madsen, W. Vermaas, S. Styring, Modified EPR spectra of the tyrosineD radical in photosystem II in site-directed mutants of *Synechocystis* sp. PCC 6803: identification of side chains in the immediate vicinity of tyrosineD on the D2 protein, Biochemistry 32 (1993) 5436–5441.
[73] A. Boussac, A.L. Etienne, Spectral and kinetic pH-dependence of fast and slow signal II in tris-washed chloroplasts, FEBS Lett. 148 (1982) 113–116.
[74] P. Faller, R.J. Debus, K. Brettel, M. Sugiura, A.W. Rutherford, A. Boussac, Rapid formation of the stable tyrosyl radical in photosystem II, Proc. Natl. Acad. Sci. U. S. A. 98 (2001) 14368–14373.
[75] P. Faller, A.W. Rutherford, R.J. Debus, Tyrosine D oxidation at cryogenic temperature in photosystem II, Biochemistry 41 (2002) 12914–12920.
[76] G. Christen, A. Seeliger, G. Renger, $P680^{+\bullet}$ Reduction kinetics and redox transition probability of the water oxidizing complex as a function of pH and H/D isotope exchange in spinach thylakoids, Biochemistry 38 (1999) 6082–6092.
[77] H. Kühne, G.W. Brudwig, Proton-coupled electron transfer involving tyrosine Z in photosystem II, J. Phys. Chem., B 106 (2002) 8189–8196.
[78] C. Berthomieu, R. Hienerwadel, A. Boussac, J. Breton, B.A. Diner, Hydrogen bonding of redox-active tyrosine Z of photosystem II probed by FTIR difference spectroscopy, Biochemistry 37 (1998) 10547–10554.
[79] M.A. Hanson, P.P. Schmidt, K.R. Strand, A. Gräslund, E.I. Solomon, K.K. Andersson, Resonance Raman evidence for a hydrogen-bonded oxo bridge in the R2 protein of ribonucleotide reductase from mouse, J. Am. Chem. Soc. 121 (1999) 6755–6756.
[80] A. Ivancich, T.A. Mattioli, S. Un, Effect of microenvironment on tyrosyl radicals. A high-field (285 GHz) EPR, resonance Raman, and hybrid density functional study, J. Am. Chem. Soc. 121 (1999) 5743–5753.
[81] R. Hienerwadel, A. Boussac, J. Breton, C. Berthomieu, Fourier transform infrared difference study of $Tyrosine_D$ oxidation and plastoquinone Q_A reduction in photosystem II, Biochemistry 35 (1996) 15447–15460.
[82] R. Hienerwadel, A. Boussac, J. Breton, B.A. Diner, C. Berthomieu, Fourier transform infrared difference spectroscopy of photosystem II $tyrosine_D$ using site-directed mutagenesis and specific isotope labeling, Biochemistry 36 (1997) 14712–14723.
[83] T. Noguchi, Y. Inoue, X.-S. Tang, Structural coupling between the oxygen-evolving Mn cluster and a tyrosine residue in photosystem II

as revealed by Fourier transform infrared spectroscopy, Biochemistry 36 (1997) 14705–14711.
[84] S.M. Beck, L.E. Brus, The resonance Raman spectra of aqueous phenoxy and phenoxy d5 radicals, J. Chem. Phys. 176 (1982) 4700–4704.
[85] G.N.R. Tripathi, R.H. Schuler, The resonance Raman of phenoxyl radicals, J. Chem. Phys. 81 (1984) 113–121.
[86] G.N.R. Tripathi, R.H. Schuler, Resonance Raman studies of substituent effects on the electronic structure of phenoxyl radicals, J. Chem. Phys. 92 (1988) 5129–5133.
[87] L.A. Kotorlenko, V.S. Aleksandrova, The vibrational spectra of neutral free radicals and the corresponding ions, Russ. Chem. Rev. 53 (1984) 1139–1153.
[88] S.A. Asher, M. Ludwig, C.R. Johnson, UV Resonance Raman excitation profiles of the aromatic amino acids, J. Am. Chem. Soc. 108 (1986) 3186–3197.
[89] C.R. Johnson, M. Ludwig, S.A. Asher, Ultraviolet resonance Raman characterization of photochemical transients of phenol, tyrosine, and tryptophan, J. Am. Chem. Soc. 108 (1986) 905–912.
[90] M.L. Mukherjee, M.L. McGlashen, T.G. Spiro, Ultraviolet resonance Raman spectroscopy and general valence force field analysis of phenolate and phenoxyl radical, J. Phys. Chem. 99 (1995) 4912–4917.
[91] M.L. McGlashen, D.D. Eads, T.G. Spiro, J.W. Whitakker, Resonance Raman spectroscopy of galactose oxidase: a new interpretation based on model compound free radical spectra, J. Phys. Chem. 99 (1995) 4918–4922.
[92] C. Berthomieu, A. Boussac, FTIR and EPR study of radicals of aromatic amino acids 4-methylimidazole and phenol generated by UV irradiation, Biospectroscopy 1 (1995) 187–206.
[93] C. Berthomieu, C. Boullais, J.-M. Neumann, A. Boussac, Effect of ^{13}C-, ^{18}O-, and ^{2}H-labeling on the infrared modes of UV-induced phenoxyl radicals, Biochim. Biophys. Acta 1365 (1998) 112–116.
[94] I. Ayala, K. Range, D. York, B.A. Barry, Spectroscopic properties of tyrosyl radicals in dipeptides, J. Am. Chem. Soc. 124 (2002) 5496–5505.
[95] J.A. Cappuccio, I. Ayala, G.I. Elliott, I. Szundi, J. Lewis, J.P. Konopelski, B.A. Barry, O. Einarsdottir, Modeling the active site of cytochrome oxidase: synthesis and characterization of a cross-linked histidine-phenol, J. Am. Chem. Soc. 124 (2002) 1750–1757.
[96] J. Spanget-Larsen, M. Gil, A. Gorski, D.M. Blake, J. Waluk, J.G. Radziszewski, Vibrations of the phenoxyl radical, J. Am. Chem. Soc. 123 (2001) 11253–11261.
[97] J. Hockertz, S. Steenken, K. Wieghardt, P. Hildebrandt, (Photo)ionization of ris(phenolato)iron(III) complexes: generation of phenoxyl radical as ligand, J. Am. Chem. Soc. 115 (1993) 11222–11230.
[98] A. Sokolowski, J. Müller, T. Weyhermüller, R. Schnepf, P. Hildebrandt, K. Hildenbrand, E. Bothe, K. Wieghardt, Phenoxyl radical complexes of zinc (II), J. Am. Chem. Soc. 119 (1997) 8889–8900.
[99] A. Sokolowski, L.H. Leutbecher, T. Weyhermüller, R. Schnepf, E. Bothe, E. Bill, P. Hildebrandt, K. Wieghardt, Phenoxyl–copper(II) complexes: models for the active site of galactose oxidase, J. Biol. Inorg. Chem. 2 (1997) 444–453.
[100] R. Schnepf, A. Sokolowski, J. Müller, V. Bachler, K. Wieghardt, P. Hildebrandt, Resonance Raman spectroscopic study of phenoxyl radical complexes, J. Am. Chem. Soc. 120 (1998) 2352–2364.
[101] S. Itoh, H. Kumei, S. Nagatomo, T. Kitagawa, S. Fukuzumi, Effects of metal ions on physicochemical properties and redox reactivity of phenolates and phenoxyl radicals: mechanistic insight into hydrogen atom abstraction by phenoxyl–radical complexes, J. Am. Chem. Soc. 123 (2001) 2165–2175.
[102] R.D. Webster, In situ electrochemical-ATR-FTIR spectroscopic studies on solution phase 2,4,6-tri-substituted phenoxyl radicals, Electrochem. Commun. 5 (2003) 6–11.
[103] W. Mäntele, Reaction-induced infrared difference spectroscopy for the study of protein function and reaction mechanisms, Trends Biochem. Sci. 18 (1993) 197–202.
[104] C. Zscherp, A. Barth, Reaction-induced infrared difference spectroscopy for the study of protein reaction mechanisms, Biochemistry 40 (2001) 1875–1883.
[105] P. Hellwig, U. Pfitzner, J. Behr, B. Rost, R.P. Pesavento, W.V. Donk, R.B. Gennis, H. Michel, B. Ludwig, W. Mantele, Vibrational modes of tyrosines in cytochrome *c* oxidase from *Paracoccus denitrificans*: FTIR and electrochemical studies on Tyr-D4-labeled and on Tyr280His and Tyr35Phe mutant enzymes, Biochemistry 41 (2002) 9116–9125.
[106] F. Tomson, J.A. Bailey, R.B. Gennis, C.J. Unkefer, Z. Li, L.A. Silks, R.A. Martinez, R.J. Donohoe, R.B. Dyer, W.H. Woodruff, Direct infrared detection of the covalently ring linked His-Tyr structure in the active site of heme-copper oxidases, Biochemistry 41 (2002) 14383–14390.
[107] D.M. Chipman, R. Liu, X. Zhou, P. Pulay, Structure and fundamental vibrations of phenoxyl radical, J. Phys. Chem. 100 (1994) 5023–5035.
[108] Y. Qin, R.A. Wheeler, Similarities and differences between phenoxyl and tyrosine phenoxyl radical structure, vibrational frequencies and spin densities, J. Am. Chem. Soc. 117 (1995) 6083–6092.
[109] Y. Qin, R.A. Wheeler, Density-functional methods give accurate vibrational frequencies and spin densities for phenoxyl radical, J. Chem. Phys. 102 (1995) 1689–1698.
[110] P.J. O'Malley, Density functional studies of phenoxyl–Na^+ ion complexes: implications for tyrosyl free radical interactions in vitro, Chem. Phys. Lett. 325 (2000) 69–72.
[111] J.M. Johnson, H.B. Halsall, W.R. Heineman, Redox activation of galactose oxidase: thin-layer electrochemical study, Biochemistry 24 (1985) 1579–1585.
[112] S. Itoh, M. Taki, H. Kumei, S. Takayama, S. Nagatomo, T. Kitagawa, N. Sakurada, R. Arakawa, S. Fukuzumi, Model complexes for the active form of galactose oxidase. Physicochemical properties of Cu(II)– and Zn(II)–phenoxyl radical complexes, Inorg. Chem. 39 (2000) 3708–3711.
[113] M. Aki, T. Ogura, Y. Naruta, T.H. Le, T. Sato, T. Kitagawa, UV resonance Raman characterization of model compounds of Tyr^{244} of bovine cytochrome *c* oxidase in its neutral, deprotonated anionic and deprotonated neutral radical forms: effects of covalent binding between tyrosine and histidine, J. Phys. Chem., A 106 (2002) 3436–3444.
[114] T. Noguchi, C. Berthomieu, Chap. 16: Molecular analysis by vibrational spectroscopy, in: T. Wydrzynski, K. Satoh, (Eds.), Photosystem II: the water/plastoquinone oxidoreductase in photosynthesis, Advances in Photosynthesis and Respiration Series, Kluwer Pub (in press).
[115] T. H.-A. Chu, N.A. Hillier, H. Law, S. Sackett, G.T. Haymond, Light-induced FTIR difference spectroscopy ofthe S2-to-S3 state transition of the oxygen-evolving complex in photosystem II, Biochim. Biophys. Acta 1459 (2000) 528–532.
[116] H.A. Chu, W. Hillier, R.J. Debus, Evidence that the C-terminus of the D1 polypeptide of photosystem II is ligated to the manganese ion that undergoes oxidation during the S1 to S2 Transition: an isotope-edited FTIR study, Biochemistry 43 (2004) 3152–3166.
[117] S. Kim, B.A. Barry, The protein environment surrounding tyrosyl radicals $D^{\bullet}$ and $Z^{\bullet}$ in photosystem II: a difference Fourier-transform infrared spectroscopic study, Biophys. J. 74 (1998) 2588–2600.
[118] S. Kim, B.A. Barry, Vibrational spectrum associated with the reduction of tyrosyl radical $D^{\bullet}$ in photosystem II: a comparative biochemical and kinetic study, Biochemistry 37 (1998) 13882–13892.
[119] I. Pujols-Ayala, B.A. Barry, Tyrosyl radicals in Photosystem II, Biochimica et Biophysica Acta 1655 (2004) 205–216.
[120] I. Ayala, S. Kim, B.A. Barry, A difference Fourier transform infrared study of tyrosyl radical Z° decay in photosystem II, Biophys. J. 77 (1999) 2137–2144.
[121] J.J. Steenhuis, B.A. Barry, Protein and ligand environments of the S2

state in photosynthetic oxygen evolution: A difference FT-IR study, J. Phys. Chem., B 101 (1997) 6652–6660.
[122] S. Kim, B.A. Barry, Reaction-induced FT-IR spectroscopic studies of biological energy conversion in oxygenic photosynthesis and transport, J. Phys. Chem., B 105 (2001) 4072–4083.
[123] G.M. MacDonald, J.J. Steenhuis, B.A. Barry, A difference infrared spectroscopic study of chlorophyll oxidation in hydroxylamine treated photosystem II, J. Biol. Chem. 270 (1995) 8420–8428.
[124] K. Onoda, H. Mino, Y. Inoue, T. Noguchi, An FTIR study on the structure of the oxygen-evolving Mn-cluster of photosystem II in different spin forms of the S2 state, Photosynth. Res. 63 (2000) 47–57.
[125] C. Berthomieu, E. Nabedryk, W. Mäntele, J. Breton, Characterization by FTIR spectroscopy of the photoreduction of the primary quinone acceptor Q_A in photosystem II, FEBS Lett. 269 (1990) 363–367.
[126] T. Noguchi, T. Ono, Y. Inoue, Detection of structural changes upon S1-to-S2 transition in the oxygen-evolving manganese cluster in photosystem II by light-induced Fourier transform infrared difference spectroscopy, Biochemistry 26 (1992) 5953–5956.
[127] C. Araga, K. Akabori, J. Sasaki, A. Maeda, T. Shiina, Y. Toyoshima, Functional reconstitution of the primary quinone acceptor, QA, in the Photosystem II core complexes, Biochim. Biophys. Acta 1142 (1993) 36–42.
[128] H. Zhang, M.R. Razeghifard, G. Fischer, T. Wydrzynski, A time-resolved FTIR difference study of the plastoquinone QA and redox-active tyrosine YZ interactions in photosystem II, Biochemistry 36 (1997) 11762–11768.
[129] Y. Kimura, T.A. Ono, Chelator-induced disappearance of carboxylate stretching vibrational modes in S2/S1 FTIR spectrum in oxygen-evolving complex of photosystem II, Biochemistry 40 (2001) 14061–14068.
[130] H.-A. Chu, M.T. Gardner, J.P. O'Brien, G.T. Babcock, Low-frequency Fourier transform infrared spectroscopy of the oxygen-evolving and quinone acceptor complexes in photosystem II, Biochemistry 38 (1999) 4533–4541.
[131] T. Noguchi, Y. Inoue, X.-S. Tang, Hydrogen bonding interaction between the primary quinone acceptor Q_A and a histidine side chain in photosystem II as revealed by Fourier transform infrared spectroscopy, Biochemistry 38 (1999) 399–403.
[132] T. Noguchi, J. Kurreck, Y. Inoue, G. Renger, Comparative FTIR analysis of the microenvironment of $Q_A^{-\bullet}$ in cyanide-treated, high pH-treated and iron-depleted photosystem II membrane fragments, Biochemistry 38 (1999) 4846–4852.
[133] A. Remy, J. Niklas, P. Kellers, T. Schott, M. Rögner, K. Gerwert, FTIR spectroscopy shows structural similarities between photosystems II from cyanobacteria and spinach, Eur. J. Biochem. 271 (2004) 563–567.
[134] D.A. Force, D.W. Randall, R.D. Britt, X.S. Tang, B.A. Diner, ^{2}H ESE ENDOR study of hydrogen bonding to the tyrosine radicals $Y_D^{\bullet}$ and $Y_Z^{\bullet}$ of photosystem II, J. Am. Chem. Soc. 117 (1995) 12643–12644.
[135] P.P. Schmidt, K.K. Andersson, A.-L. Barra, L. Thelander, A. Gräslund, High field EPR studies of mouse ribonucleotide reductase indicate hydrogen bonding of the tyrosyl radical, J. Biol. Chem. 271 (1996) 23615–23618.
[136] O. Nwobi, J. Higgins, X. Zhou, R. Liu, Density functional calculation of phenoxyl radical and phenolate anion: an examination of the performance of DFT method, Chem. Phys. Lett. 272 (1997) 155–161.
[137] P.J. O'Malley, Density functional calculations modeling tyrosine oxidation in oxygenic photosynthetic electron transfer, Biochim. Biophys. Acta 1553 (2002) 212–217.
[138] F. Himo, A. Gräslund, L.A. Eriksson, Density functional calculations on model tyrosyl radicals, Biophys. J. 72 (1997) 1556–1567.
[139] P.J. O'Malley, D. Ellson, The calculation of ^{1}H, ^{13}C, ^{14}N isotropic and anisotropic hyperfine interactions for the 3-methyl indole cation and neutral radicals using hybrid density functional methods: models for in vivo tryptophan-based radicals, Biochim. Biophys. Acta 1320 (1997) 65–72.
[140] A. Mezzetti, A.L. Maniero, M. Brustolon, G. Giacometti, L.C. Brunel, A tyrosyl radical in an irradiated single crystal of *N*-acetyl-L-tyrosine studied by X-band cw-EPR, high-frequency EPR, and ENDOR spectroscopies, J. Phys. Chem., A 103 (1999) 9636–9643.
[141] E.L. Fasanella, W. Gordi, Electron spin resonance of irradiated single crystals of L-phenylalanine–HCl, Proc. Natl. Acad. Sci. U. S. A. 62 (1969) 299–304.
[142] G.J. Gerfen, B.F. Bellew, S. Un, J.M. Bollinger, J. Stubbe, R.G. Griffin, D.J. Singel, High-Frequency (139.5 GHz) EPR Spectroscopy of the Tyrosyl Radical in *Escherichia coli* ribonucleotide reductase, J. Am. Chem. Soc. 115 (1993) 6420–6421.
[143] S. Un, M. Atta, M. Fontecave, A.W. Rutherford, g-Values as a Probe of the Local Protein Environment: High-Field EPR of Tyrosyl Radicals in Ribonucleotide Reductase and Photosystem II, J. Am. Chem. Soc. 117 (1995) 10713–10719.
[144] S. Un, X.S. Tang, B.A. Diner, 245 GHz high-field EPR study of tyrosine-$D^{\bullet}$ and tyrosine-$Z^{\bullet}$ in mutants of photosystem II, Biochemistry 35 (1996) 679–684.
[145] S. Un, C. Gerez, E. Elleingand, M. Fontecave, Sensitivity of tyrosyl radical g-values to changes in protein structure: a high-field EPR study of mutants of ribonucleotide reductase, J. Am. Chem. Soc. 123 (2001) 3048–3054.
[146] Y. Kimura, K. Hasegawa, T. Ono, Characteristic changes of the S2/S1 difference FTIR spectrum induced by Ca^{2+} depletion and metal cation substitution in the photosynthetic oxygen-evolving complex, Biochemistry 41 (2002) 5844–5853.
[147] H.-A. Chu, W. Hillier, N.A. Law, G.T. Babcock, Vibrational spectroscopy of the oxygen-evolving complex and of manganese model compounds, Biochim. Biophys. Acta 1503 (2001) 69–82.
[148] P. Allard, A.-L. Barra, K.K. Anderson, P.P. Schmidt, M. Atta, A. Gräslund, Characterization of a new tyrosyl free radical in *Salmonella typhimurium* ribonucleotide reductase with EPR at 9.45 and 245 GHz, J. Am. Chem. Soc. 118 (1996) 895–896.
[149] C.W. Hoganson, M. Sahlin, B.-M. Sjöberg, G.T. Babcock, Electron magnetic resonance of the tyrosyl radical in ribonucleotide reductase from *Escherichia coli*, J. Am. Chem. Soc. 118 (1996) 4672–4679.
[150] P.J. van Dam, J.-P. Willems, P.P. Schmidt, S. Pötsch, A.-L. Barra, W.R. Hagen, B.M. Hoffman, K.K. Anderson, A. Grässlund, High-frequency EPR and pulsed Q-band ENDOR studies on the origin of the hydrogen bond in tyrosyl radicals of ribonucleotide reductase R2 proteins from mouse and herpes simplex virus type 1, J. Am. Chem. Soc. 120 (1998) 5080–5085.
[151] B.S. Selinsky, K. Gupta, C.T. Sharley, P.J. Loll, Structural analysis of NSAID binding by prostaglandin H2 synthase: time-dependent and time-independent inhibitors elicit identical enzyme conformations, Biochemistry 40 (2001) 5172–5180.
[152] T. Tamada, K. Kitadokoro, Y. Higuchi, K. Inaka, A. Yasui, P.E. de Ruiter, A.P. Eker, K. Miki, Crystal structure of DNA photolyase from *Anacystis nidulans*, Nat. Struct. Biol. 4 (1997) 887–891.